

## Article

# Spin-Mechanics with Nitrogen-Vacancy centers and trapped particles

Maxime Perdriat <sup>1</sup>, Clément Pellet-Mary <sup>1</sup>, Loïc Rondin <sup>2</sup> and Gabriel Hétet <sup>1,\*</sup>

<sup>1</sup> Laboratoire De Physique de l'École Normale Supérieure, École Normale Supérieure, PSL Research University, CNRS, Sorbonne Université, Université de Paris , 24 rue Lhomond, 75231 Paris Cedex 05, France

<sup>2</sup> Affiliation 2

\* gabriel.hetet@ens.fr

**1** **Abstract:** The motion of an optically trapped silica sphere has been cooled to the ground state of motion last year, showing the potential of levitating nano-particles to realize quantum mechanical experiments at room temperature. Adding spin degrees of freedom to the toolbox would enable accessing a very rich playground at the crossroad between condensed matter and atomic physics and with prospects for exploring quantum effects and improved sensors based on the laws of quantum mechanics. We review recent experimental and theoretical work in the field of spin-mechanics that employ the interaction between trapped crystals and electronic spins in the solid state. We discuss the challenges that the manipulation of spins in levitating particles as well as other approaches where the spins are coupled distantly to the magnet. The current experiments are limited to high temperature, so we treat the motional degrees of freedom classically. When dealing with naturally anisotropic crystals, the natural degree of freedom that emerges is the angular motion and the torque given by spins with a natural quantization axis. We therefore discuss in more details the coupling between the so-called librational motion the spins. We also discuss perspectives for sensing and for cooling in the classical regime of the mechanical oscillator.

**15** **Keywords:** Nitrogen-Vacancy centers; micro-mechanical oscillators; electronic spin resonance

## **16** 1. Introduction

**17** The unique control offered by single quantum systems, such as atoms or ions, has  
**18** enabled an immense boost in the developments of quantum technologies. Extending  
**19** these technologies to larger masses could also reveal exciting, both for fundamental  
**20** question on the nature of quantum physics at larger scale, and for the development of  
**21** innovative sensors such as exquisite force sensors and accelerometers.

**22** Electro-, magneto- or opto- mechanically controlled levitating objects under vacuum  
**23** are fascinating in this regard and have been at the heart of intense research activities  
**24** lately. This attention is supported by the exquisite control that one can exert onto  
**25** the levitated objects as opposed to tethered systems. Beyond the natural exceptional  
**26** isolation they offer, these platforms allow addressing numerous degrees of freedom,  
**27** easy tuning of the trapping potential, as well as free-fall experiments. The promises  
**28** of this research field have been supported by recent experiments. Recent works have  
**29** reported trapped particles in the quantum regime [1,2], while active development of  
**30** force sensors and tests of fundamentals physics models have been proposed [3–5].

**31** To push forward these developments, and by analogy with the long expertise of  
**32** atomic and molecular optics communities, coupling the dynamics of the levitated system  
**33** to a single intrinsically quantum system, such as an ion, atoms, or equivalent artificial  
**34** atoms have been proposed.

**35** Controlling the motion of macroscopic systems using individual atomic spins has  
**36** long been a driving force in research on quantum physics. One archetypical example is

**Citation:** Title. *Journal Not Specified* 2021, 1, 0. <https://doi.org/>

Received:

Accepted:

Published:

**Publisher's Note:** MDPI stays neutral with regard to jurisdictional claims in published maps and institutional affiliations.

**Copyright:** © 2021 by the authors. Submitted to *Journal Not Specified* for possible open access publication under the terms and conditions of the Creative Commons Attribution (CC BY) license (<https://creativecommons.org/licenses/by/4.0/>).

the field of cold trapped ions, where the interaction between distant electronic spins is mediated by the collective ion motion. Fueled by the major implications in quantum information, sensing and simulation, a wide variety of other platforms are being explored, in which the atomic qubits are interacting through other degrees of freedom, such a single photons or with ancilla spin qubits. Inspired by pioneering accomplishments in atomic-physics, the recent developments in the field of spin-mechanics now also provide pathways for quantum experiments with macroscopic objects. Indeed, it is for example possible to operate mechanical oscillators close to the motional quantum ground state and to envision using their motion a bus for distributing entanglement amongst many spins.

This system will provide unique platforms for fundamental tests of quantum mechanics at the crossroad between condensed matter and atomic physics, paving the way towards nano-scale magnetism with long-lived and controllable spins in a solid. Last, it will fuel energy into the field of quantum metrology *via* quantum enhanced gyroscopy and matter-wave interferometry. Such coupling could provide important advantages for quantum sensing and metrology by providing enhanced the measurement sensitivity. It could also provides an additional non-linearity and/or control that could be helpful to build non classical states of the motion. Finally, they could also serve as transducers between optical or RF signal to the mechanical mode.

In this paper, we first describe the state of the art levitation systems and their specificities. Then we ... The special case of NV defect in diamond will be discussed thoroughly, due to its prevalence in recent experiments.

## 2. Trapping particles

The basic idea behind particle levitation is to use a field to hold a particle in air or vacuum against gravitation. In the context of levitation under vacuum environments, electromagnetic fields, such as optical fields, RF electric fields, or magnetic fields are used. Despite its growing interest, we will not consider acoustic levitation since it does not apply under vacuum conditions.

The original proposals suggested using optical forces. Under laser illumination, small dielectric particles become polarized. The strongest fields then attract the induced dipole. The particles can be stably trapped in three dimensions, either at the focus of a laser beam, i.e., optical tweezers configuration [6] (Fig. 1-(a)), in a node of a cavity field [7] or in the near-field of photonic crystal [8]. Reference [9] presents a broad insight into optical tweezers.

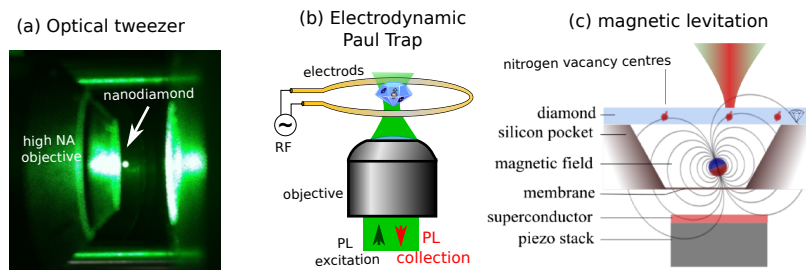


**Figure 1.** Different approaches to particle levitation. (a) Optical tweezer. A strongly focused infrared laser through a high numerical aperture (NA) objective (on the left) allows to trap a nanodiamond at its focus. The strong scattering of the green laser used for PL excitation allows to see the nanodiamond with the bare eye. (b) Electrodynamics Paul trap : a charged diamond particle is held under vacuum by electric field gradients. (c) Magnetic levitation. A magnetic particle is levitated above a superconductors. NV centres implanted in a diamond slab above the levitated particle can be coupled to its motion through the magnetic field gradient. Adapted from ref [10].

71 An alternative, described in figure 1-(b), uses electrodynamics traps, typically  
 72 Paul quadrupole traps, to levitate charged particles. The radio-frequencies modulation  
 73 of the high voltage electric field between the trap electrodes ensures the particle's  
 74 three-dimensional confinement. Finally, diamagnetic traps use static magnetic fields to  
 75 levitate either standard diamagnetic or superconducting particles. Since static magnetic  
 76 fields do not allow three-dimensional confinement, magnetic traps generally work  
 77 against gravity to get vertical confinement. Also, note that the position of the magnetic  
 78 and the diamagnetic object is arbitrary. One can levitate a magnetic object above a  
 79 diamagnetic/superconductor holder, or a diamagnetic particle can be levitated above  
 80 magnets. Other types of levitation schemes include inductive-levitation or schemes  
 81 that use feedback like the Abel trap or inductive... but are seldom employed to levitate  
 82 microscopic objects.

Since the physics of these different approaches differs, their exact properties and abilities will be strongly setup dependent. The dynamics of a levitated particle, along a given direction, parametrized by the coordinate  $q$ , can be almost often described by the Langevin equation:

$$\frac{d^2q}{dt^2} + \gamma \frac{dq}{dt} = \frac{F_{\text{trap}} + F_{\text{fluct}}}{m}, \quad (1)$$

83 with  $\gamma$  the translational damping,  $F_{\text{trap}}$  the trapping force that allows the particle to  
 84 levitate and  $F_{\text{fluct}}$  is the fluctuation force, induce by the interaction between the particle  
 85 and the gas molecule. Usual rarefied gas can be described as a Markovian thermal bath  
 86 with a white noise spectrum, and thus the fluctuation force is described by  $\langle F_{\text{fluct}} \rangle = 0$ ,  
 87 and  $\langle F_{\text{fluct}}(t)F_{\text{fluct}}(t') \rangle = 2\gamma k_B T \delta(t - t')$ . Interestingly, while the value of  $\gamma$  depends on  
 88 the exact shape of the particle [11], it scales as the inverse of the residual gas pressure  
 89  $P_{\text{gas}}$  and of the characteristic size of the particle. This is actually one property that make  
 90 levitation attractive, since thermal noise can be made arbitrary small, just by reducing  
 91 the gas pressure inside the vacuum chamber.

The exact form of  $F_{\text{trap}}$  will obviously depends on the used levitation approach. However, for a particle stably trapped around a given position, one can linearized the trapping force, and the particle dynamics is then described by an harmonic oscillator, with

$$F_{\text{trap}} = -m\Omega_q^2 q,$$

92 where  $m$  is the particle mass, and  $\Omega_q$  the angular frequency of the trap. The expected  
 93 value of this parameter for the different approaches is presented in table ???. Note that in  
 94 practice the dynamics of the particle may appears more complex than a simple harmonic  
 95 oscillator and that non-linearities [12] or supplementary forces has to be accounted  
 96 for [13].

97 In general the studied motion is the three translations of the particle, and the  
 98 coordinate  $q$  is actually one of the Cartesian coordinates  $x, y$  or  $z$ . But, both due to fact  
 99 that levitodynamics deals with solid body, and the ease of access to various dynamics,  
 100 other degrees of freedom can easily be access, specifically rotation. Equation 1 can be  
 101 straightforwardly be adapted to rotation, by accounting of angular momentum, and be  
 102 recasted in the same form by paying attention to change forces to torques. In the context  
 103 of levitodynamics, two rotational dynamics have been observed, pure rotation [14–17],  
 104 with rotation frequencies up to a few GHz, and a librational mode (also sometimes called  
 105 torsional mode). These new modes are specifically interesting in the context of hybrid  
 106 spin-levitodynamics systems, where they offers new coupling modalities as it will be  
 107 discussed in the following.

### 108 3. Coupling to an ancillary quantum systems

#### 109 3.1. Intro : problematic

110 As discussed in the introduction, coupling the levitated object to an ancillary  
 111 quantum systems is an exiting way to extend it capabilities.

112 The first quantum systems to consider are atoms or ions, as in traditional atomic  
113 and molecular optics (AMO) experiments. Such approaches have been proposed theoretically [18] and demonstrated for clamped optomechanics [19,20]. However, due to the  
114 raised technical challenges, "solid state atoms-like" represents an exciting alternative. For  
115 instance, it is possible to levitated colloidal quantum dots [21], rare-earth ions in a solid  
116 matrix [22], or color centres in semi-conductors particles [23–25] (e.g. diamond, SiC,  
117 silicon). The motion of a levitated magnetic can also be coupled to a superconducting  
118 qubits... These objects being hosted in a solid-state matrix can be easily manipulated and  
119 embedded in a levitated system, keeping experimental complexity simple.

120  
121 Coupling an spin to the motion of objects have been looked at already in various  
122 platforms.

123 Through these different systems, the second criterium of choice is the possible  
124 coupling mechanisms between the ancillary systems' quantum state and the levitated  
125 particles' dynamics for one or more degrees of freedom. A usual mechanism for this  
126 coupling is the Zeeman effect, which may couple the atomic-like system's internal degree  
127 of freedom to the particle motion through a position or velocity dependent magnetic  
128 field. Equivalently the Stark effect provides an equivalent coupling using electric fields.  
129 The strength of these mechanisms will depend on the considered system.

130 In this context, NV color centers in diamond are of particular interest. First, due to  
131 the intense research activities around these color centers, triggered by its potential in  
132 quantum information processing and the development of innovative sensors. Thus, our  
133 understanding of NV centers' properties and our control on the diamond materials have  
134 grown heavily over the last decade. Second, the NV centers' spin properties can easily  
135 be coupled to the diamond host matrix's motion using a magnetic field. This aspect is  
136 even strengthened in levitodynamics, where librational modes of the diamond can be  
137 efficiently coupled to the NV spin states, as will be discussed in the following. We thus  
138 discuss mostly NV centers here, but the presented methods could extend to other color  
139 centres, notably in SiC, where similar spin properties have been reported.

### 140 3.2. Coupling the motion of levitating particles to spins : the special case of NV centers

141 Physics and applications of NV color centers have already been widely discussed  
142 in recent reviews [26], we just remind here basics of NV physics in the context of levito-  
143 dynamics.

144  
145 The NV color centre is a point defect of the diamond matrix consisting of a substitutional  
146 nitrogen atom (N) combined with a vacancy (V) in one of the nearest neighbouring sites  
147 of the diamond crystal lattice as depicted in figure 2-(a). This defects behaves as an  
148 artificial atoms hosted by the diamond matrix. It combines unique luminescence and  
149 spin properties that are at the heart of the intense research activity around this point  
150 defect.

151 Indeed NV centre owns an extremely stable luminescence in the near-infrared  
152 (its zero-phonon lines is around  $\lambda_{ZPL} = 637$  nm and is associated with broad phonon  
153 sideband). This luminescence can be accessed at the single center level using standard  
154 confocal microscopy. In addition the NV centre ground state is a spin triplet  $S = 1$ , with  
155 a quantification axis  $\vec{u}_{NV}$  enforced by the N – V axis of the defect. The spin projection  
156 along this axis are noted with the quantum number  $m_s$ . Due to a spin-spin interaction  
157 the  $|m_s = \pm 1\rangle$  states are split from the  $|m_s = 0\rangle$  by the zero-field splitting parameter  
158  $D \approx 2.88$  GHz (see Fig. 2-(b)). Note that in strained diamond the states  $|m_s = \pm 1\rangle$  can  
159 also be split, by a parameters often noted  $2E$ . Typically in nanodiamonds this splitting is  
160 of a few MHz. In practice it makes the NV centre less sensitive to small magnetic fields,  
161 a drawback that can be overcome using a magnetic bias field. Thus in the following we  
162 will neglect this strain induced zero-fields splitting.

163 One interesting aspect of NV centres, is the opportunity to optically initialise  
164 and read its spin state. Indeed, under laser irradiation the NV centre is polarised

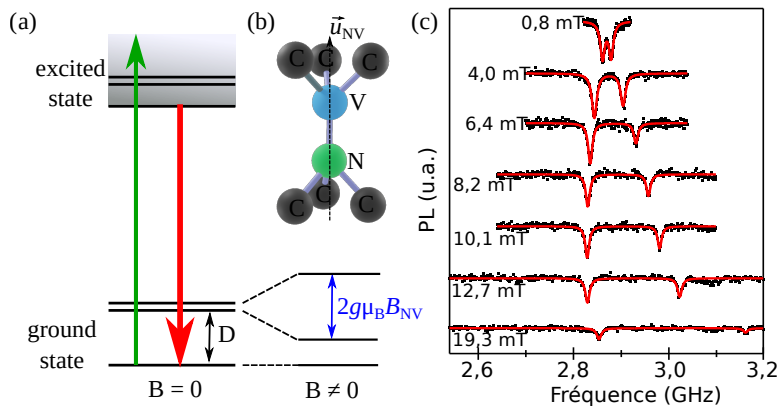


**Figure 2.** NV centre photophysics. (a) Simplified electronic structure of the NV colour centres. (b) Schematic of the crystalline structure of NV defect in diamond. The axis  $N - V$  is the quantification axis. (c) Exemple of optically detected magnetic resonance on a single NV center in a bulk diamond. The magnetic field is applied with an angle  $\theta = 74^\circ$  with respect to the NV axis. Adapted from [27]

in the  $|m_s = 0\rangle$  state, while the photoluminescence levels depends on the considered level. The  $|m_s = 0\rangle$  state being up to 50 % brighter than the  $|m_s = \pm 1\rangle$  states. This constitute the basis of *Optically Detected Magnetic Resonance* (ODMR), where we record the photoluminescence of the NV centre as a function of the frequency of an applied microwave field. A drop of luminescence is observed when the microwave is resonant with one of the transitions from  $|m_s = 0\rangle$  to  $|m_s = \pm 1\rangle$ . Typical ODMR spectra are presented in figure 2-(c).

Under a magnetic field, due to the Zeeman effect, the states  $|m_s = \pm 1\rangle$  split. For small magnetic fields, typically  $B \ll 10$  mT, the observed splitting is

$$\Delta\nu_{\pm} = 2g\mu_B B_{NV} \quad (2)$$

with  $g$  the Landé Factor,  $\mu_B$  the Bohr magneton and  $N_{NV}$  the magnetic field projection along the  $N - V$  axis. For larger magnetic field, to determine the exact splitting one have to account for the Hamiltonian of the NV ground state:

$$H/\hbar = \quad (3)$$

Change with respect to angle. PLOTS.

The Zeeman induce splitting is actually an efficient way to couple the motion of a levitated diamond to the NV spin states that it hosts. Initial proposals, based on clamped optomechanics proposed to coupled the displacement of the mechanical resonator to NV spin using a magnetic field gradient. While this approach have been successfully applied to the mechanical detection of nano magnetic resonance, and used to coupled levitated magnetic beads to NV centres [10], reaching the strong magnetic field gradients required for important spin-mechanics coupling is experimentally challenging. Interestingly, levitodynamics offers an interesting alternative while considering the libration of the levitated particle, that can be coupled to embedded NV spins through static magnetic fields [28]. These question will be discussed in details in paragraph XXX.

Note that coupling via strain or electrical fields is also possible, since it also leads to a splitting of the spins states. However electric coupling for NV centres is much weaker than magnetic coupling and also more complex to implement in the context of levitodynamics.

### 3.3. Characterisation of NV centres

The huge progresses on material engineering have enabled a great level of controls on the properties of the NV centres

190      Numbers of NV centres

191      A first parameters of importance is the number of NV centres involved in the  
 192      experiment. First, increasing the numbers of NV centres leads to an increase of the  
 193      collected photoluminescence and of the signal to noise ratio, an so of the sensitivity  
 194      of the measurement as discussed previously *TODO?*. Additionally this also strengthen  
 195      the coupling between the spin states of the ensemble and the diamond motion, that  
 generally grows as  $\sqrt{N}$  with  $N$  the number of involved spins *TO CHECK, and references*.

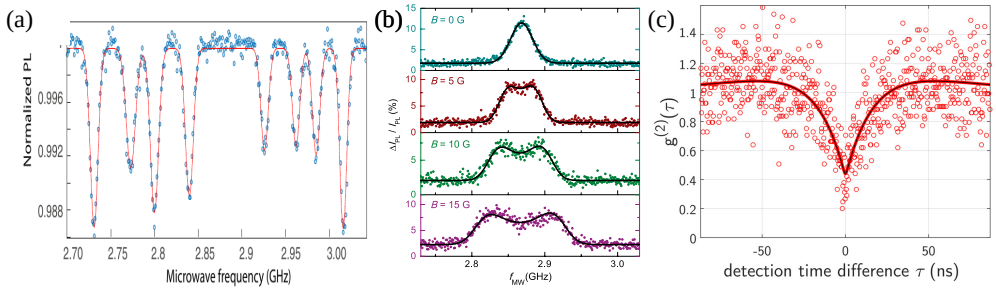


Figure 3. (a) ODMR spectrum for a small ensemble of NV centres in a levitated microdiamond under magnetic fields. Height peaks, corresponding to the four orientations of the NV centers, are observed. Adapted from ref [24]. (b) ODMR for small ensembles of nanodiamond trapped in water, under increasing magnetic fields. Adapted from [29]. (c) Autocorrelation of photon emission in a levitated nanodiamond. The antibunching deep at zero delay, below 0.5 is a proof of the presence of a single NV center. Adapted from [13].

196      However working with spin ensemble may be detrimental. The first potential  
 197      drawback is that spins at different positions or orientations will couple differently to the  
 198      magnetic field, and thus lead to inhomogeneous broadening of the coupling strength. In  
 199      addition, spin properties of NV ensemble are generally worse than the one achievable  
 200      with single NV centres. Finally, multiple NV orientations may complicate some exper-  
 201      imental implementation of protocols. If under some diamond growth conditions it is  
 202      possible to favor NV ensemble with a defined orientation [?], for usual monocrystalline  
 203      diamond NV centres have four different orientations corresponding to the four possible  
 204      crystalline orientation in the diamond lattice. This is clearly observed while performing  
 205      ODMR on a NV ensemble under a sufficient bias field, as shown in figure 3, where four  
 206      sets of resonance are clearly visible. Note that if the diamond is rotating, the ODMR  
 207      spectrum becomes even harder to interpret, since all the lines mix (Fig. 3-(b)).

208      Note that for NV centres ensemble, precise estimation of the NV density is not  
 209      straightforward. Generally, we assumed it by comparing the total collected luminescence  
 210      to the luminescence of a single NV centres under the same condition. *est ce que c'est bien*  
 211      *documenté dans la littérature, papier sur le T2 aussi?*

212      In the case, where we want to limit the drawback associated with large ensemble  
 213      of NV centres, we can certify that there is only one NV center hosted in the diamond  
 214      of interest, using standard quantum optics techniques, i.e. photon autocorrelation  
 215      measurement. Using Hanbury Brown and Twiss interferometer, we can assure that the  
 216      photons are emitted one after the other, a proof of the singleness of the emitters. This  
 217      singleness translates as a dip for zero delay in the autocorrelation function  $g^{(2)}(0) <$   
 218      0.5, as shown in figure *TODO*. Single NV centres have been levitated using optical  
 219      tweezers [23,30] and Paul traps [13]. In addition, Gieseler et al. demonstrated the  
 220      coupling of single NV centres in a bulk diamond slab and a levitated magnetic beads.  
 221      This approach is interesting since it uses NV centres in bulk diamond, where NV spin  
 222      properties can be extremely well controlled.

223      Note, that if required the orientation of a given NV centres can be measured by  
 224      applying a calibrated magnetic field, and recording the associated ODMR spectrum [26].

<sup>226</sup> Spin properties: coherence and relaxation

<sup>227</sup> The coupling by itself would not be the only figure of merits, and to exploits it it is  
<sup>228</sup> important to The properties of the quantum systems will play an important role on its  
possible usage, A quantum system, prepared in a given pure state will change state

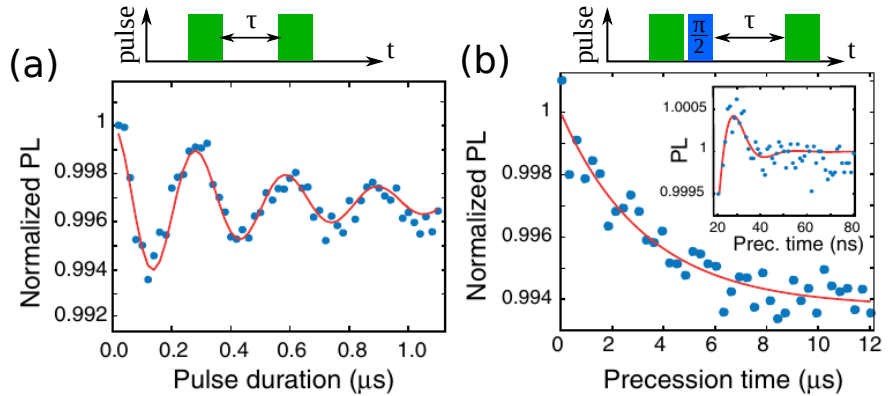


**Figure 4.** Characterisation of spin properties of NV centres. Rabi oscillations (a) and spin echo (b) of a small ensemble of NV centers in a levitated microdiamond. Adapted from [24].

<sup>229</sup> A mechanical analogy can be made where the damping rate is analogous to the  
<sup>230</sup> relaxation rate  $1/T_1$  and the lost of coherence of a mechanical mode, for instance due to  
<sup>231</sup> frequency fluctuation will be analogue to  $1/T_2$ .

<sup>232</sup> The time can be  
<sup>233</sup> This different time scale

<sup>234</sup>

### 3.3.1. Number of NV centres

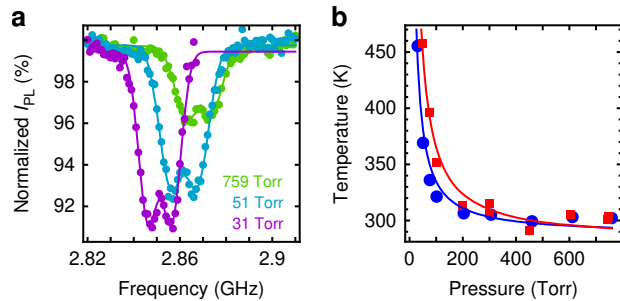


**Figure 5.** Effect of pressure on ESR: heating *soit ici, soit dans le dernier chapitre*

<sup>235</sup>

## 4. Description of the system

<sup>236</sup> We consider a levitating diamond containing a single NV center in a presence  
<sup>237</sup> of a magnetic field. we will discuss the one-dimensional situation where one angle  
<sup>238</sup> is controlled by a single spin using a homogeneous magnetic field and where one  
<sup>239</sup> coordinate in space is controlled by a single spin using a gradient of a magnetic field. We  
<sup>240</sup> will first estimate the resulting force and torque in different experimentally accessible  
<sup>241</sup> situations and then consider the influence of a microwave tone. We will show that even  
<sup>242</sup> in the presence of a magnetic field gradient or a homogeneous magnetic field, the spin  
<sup>243</sup> can exert a significant confining force/torque due to the spin-spring effect. Then we  
<sup>244</sup> evaluate analytically the spin-cooling of the librational and the center of mass motion  
<sup>245</sup> and discuss the limits to cooling.

<sup>246</sup>

**247 5. Hamiltonian of the spin-mechanical system**

**248** We will study the coupling between a single spin and the two main degrees of  
**249** freedom of a levitating mechanical oscillator: the center of mass motion (CoM) and  
**250** the libration. We will assume that there is no coupling between these two degrees of  
**251** freedom so that we can treat it separately. This may not be true generally. For instance,  
**252** in Paul traps, if the charge distribution contains a non-zero dipole component, the center  
**253** of mass and the angle may become coupled [1]. In optical tweezers, this may be the case  
**254** if? Because of non-inertial frame effects as well as the presence of a transverse magnetic  
**255** field needed to entail the spin coupling, the spin-librational coupling physics is richer.

**256 5.1. Coupling to the center of mass**

**257 5.1.1. System and origin of the coupling**

**258** In this part, we assume that the three degrees of freedom of the CoM motion are not  
**259** coupled via the trapping mechanism so that we can reduce the study of the spin-CoM  
**260** coupling to a 1D problem. We assume that the NV axis is given along the direction  
**261** of the magnetic field  $z$ . The CoM motion will be treated classically. Furthermore, we  
**262** suppose the magnetic field gradient to be in the  $z$  direction so that  $\vec{B} = B_0 \vec{e}_z + \frac{\partial B_z}{\partial z} z \vec{e}_z$  to  
**263** first order in the position operator. Under those assumptions, the Hamiltonian of the  
**264** spin-mechanical system reads

$$\hat{\mathcal{H}}_{\text{com}} = \frac{p_z^2}{2m} + \frac{1}{2} m \omega_z^2 z^2 + \hbar D \hat{S}_z^2 + \hbar \gamma_e B_0 \hat{S}_z + \hbar \gamma_e \frac{\partial B_z}{\partial z} z \hat{S}_z \quad (4)$$

**265** The magnetic states are the eigenstates of  $\hat{S}_z$  spin operator so the magnetic energy  
**266** is linearly proportional to the particle position as represented in Fig 1 (à faire avec  
**267** l'évolution des niveaux d'énergies en fonction de  $z$  et aussi en fonction de theta pour la  
**268** libration). A magnetic force directly related to the magnetic field gradient and the spin  
**269** polarisation can thus be applied to the particle.

**270 5.1.2. Experimental consideration**

Let us discuss the magnetic force and the required magnetic field gradient in order to reach a sizable displacement.

$$F_s = - \left\langle \frac{\partial \hat{\mathcal{H}}_{\text{com}}}{\partial z} \right\rangle = - \hbar \gamma_e \frac{\partial B_z}{\partial z} \langle \hat{S}_z \rangle = - \hbar \gamma_e \frac{\partial B_z}{\partial z} (\rho_{1,1} - \rho_{-1,-1}). \quad (5)$$

**271** where  $\rho_{1,1} = \langle +1|+1 \rangle$  and  $\rho_{-1,-1} = \langle -1|-1 \rangle$  Assuming that the Paul trap confinement  
**272** frequency is  $\omega_z$  and a particle with a mass  $m$ , the shift in the oscillator position in a  
**273** magnetic state is

$$\Delta z = \frac{\hbar \gamma_e}{m \omega_z^2} \frac{\partial B_z}{\partial z} \quad (6)$$

**274** Assuming a 15 micron size particle in a Paul trap, containing  $10^9$  NV centers. The  
**275** mass of such a diamond is  $m = 0.5 \times 10^{-12}$  kg. Taking  $\omega_z = 2\pi \times 100$  Hz, we get an  
**276** order of magnitude displacement of

$$\Delta z = 10^{-11} \frac{\partial B_z}{\partial z} [m] \quad (7)$$

**277** with  $\frac{\partial B_z}{\partial z}$  expressed in G/m.

**278** Using a modest 10 T/m gradient, we get a displacement of 1  $\mu\text{m}$ . This is readily  
**279** measurable. Such a force from NV centers has not been observed so far.

**280** One difficulty is to align the magnetic field along the [111] direction. There will  
**281** otherwise be torques applied to the particle, which may mask the coupling to the CoM

<sup>282</sup> mode. Let us now discuss the coupling between the spin and the angular degree of  
<sup>283</sup> freedom.

<sup>284</sup> 5.2. *Coupling to the libration*

<sup>285</sup> 5.2.1. System and origin of the coupling

<sup>286</sup> The diamond is supposed to be spherical so that the inertia  $I$  is the same in the  
<sup>287</sup> three directions of space.

<sup>288</sup> As depicted in Fig1 (à faire), the directions of the laboratory frame are given by  
<sup>289</sup>  $(0, \vec{e}_x, \vec{e}_y, \vec{e}_z)$ . The direction of the diamond is given by the  $(0, \vec{e}_{x'}, \vec{e}_{y'}, \vec{e}_{z'})$  where  $z'$  gives  
<sup>290</sup> the anisotropy axis of the NV center in the crystalline structure of the diamond. The  
<sup>291</sup> three Euler angles operators  $(\hat{\phi}, \hat{\theta}, \hat{\psi})$  describing the angular position of the diamond are  
<sup>292</sup> chosen in the  $(zy'z'')$  convention. The magnetic field direction is supposed to be fixed in  
<sup>293</sup> the laboratory frame and is given along the  $z$  direction so that  $\vec{B} = B\vec{e}_z$ .

<sup>294</sup> The Hamiltonian of the spin-mechanical system in the laboratory frame reads

$$\hat{\mathcal{H}}_{\text{lib}} = \frac{\hat{L}^2}{2I} + U(\hat{\phi}, \hat{\theta}, \hat{\psi}) + \hbar D \hat{S}_{z'}^2 + \hbar \gamma_e B \hat{S}_z \quad (8)$$

<sup>295</sup> where  $\hat{L}$  is the angular momentum operator of the diamond in the laboratory frame,  
<sup>296</sup>  $U(\hat{\phi}, \hat{\theta}, \hat{\psi})$  is the confining potential given by the Paul trap and  $\hat{S}_z, \hat{S}_{z'}$  are NV center spin  
<sup>297</sup> operators.

<sup>298</sup> Few remarks can be made about this Hamiltonian. Contrary to the CoM spin-  
<sup>299</sup> mechanical coupling [cite], one has to be careful that the NV direction given by  $z'$  is  
<sup>300</sup> not fixed in the laboratory frame. This implies that the  $\hat{S}_{z'}$  operator depends on the  
<sup>301</sup> angular operators  $(\hat{\phi}, \hat{\theta}, \hat{\psi})$  which do not commute with the diamond angular momentum  
<sup>302</sup> operator  $\hat{L}$ . Consequently, the commutator  $[\hat{L}^2, \hat{S}_{z'}^2]$  is not equal to zero. It allows a  
<sup>303</sup> coupling between the angular motion of the diamond and the NV center responsible for  
<sup>304</sup> effects as macroscopic torque on the diamond. The coupling origin of the libration with  
<sup>305</sup> the spin is thus different from the CoM coupling which directly comes from the Zeeman  
<sup>306</sup> term.

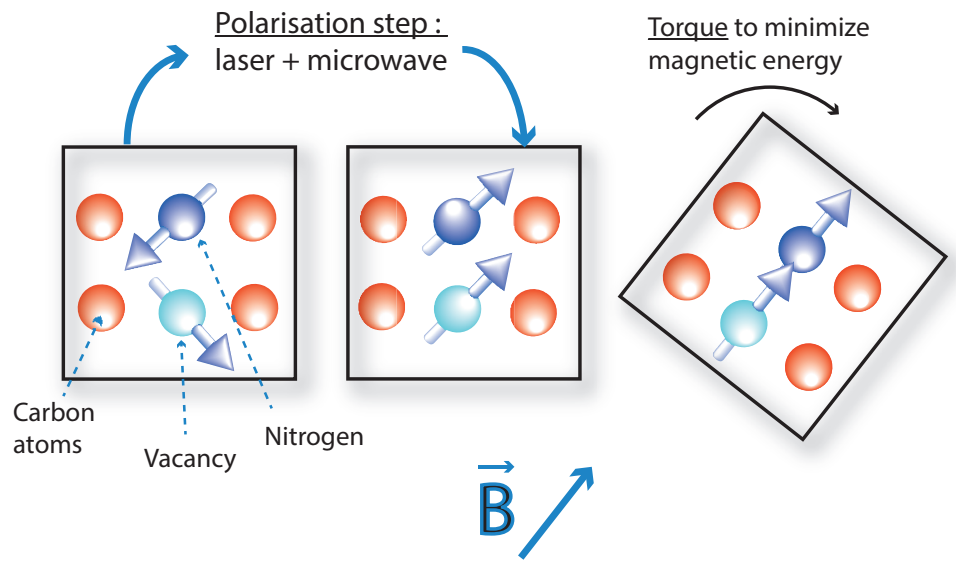
<sup>307</sup> Theoretically, the presence of the magnetic field is not required to see effects from  
<sup>308</sup> the spin-libration coupling [cite]. We can cite the Einstein-de Haas effect which comes  
<sup>309</sup> from the angular momenta exchange between a spin and a macroscopic rotor.

<sup>310</sup> However, the spin-libration coupling we are interested in is only activated by the  
<sup>311</sup> presence of a magnetic field. A simple image of this coupling is that the excited states  
<sup>312</sup> act as magnetic dipoles when polarized. Thus, polarizing the NV center in an excited  
<sup>313</sup> state makes it sensitive to the magnetic field. Due to the spin-coupling with the libration,  
<sup>314</sup> it makes the whole diamond sensitive to the magnetic field which can rotate in order to  
<sup>315</sup> minimize the magnetic energy of the spin exactly as a hard magnet. A brief picture of the  
<sup>316</sup> full interaction is shown in Fig 2.

<sup>317</sup> 5.2.2. Simplified Hamiltonian

Even if the coupling origin is well-described, the current Hamiltonian doesn't make it appear clearly as in the CoM coupling. In the following, we will restrict the study of the spin-librational coupling to one librational mode that is supposed to be in the spin-magnetic field plane given by the  $(xy)$  plane. The diamond angular motion is parametrized by the nutation angle operator  $\hat{\theta}$ . We introduce the notation  $\theta'$  for the equilibrium angular position of the diamond given by the Paul trap. The Hamiltonian of the simplified system reads

$$\hat{\mathcal{H}}_{\text{lib}} = \frac{\hat{\theta}_\theta^2}{2I} + \frac{1}{2} I \omega_\theta^2 (\hat{\theta} - \theta')^2 + \hbar D \hat{S}_{z'}^2 + \hbar \gamma_e B \hat{S}_z. \quad (9)$$

**Figure 6.** Spin-torque

Moving to the particle frame through the unitary transformation  $\hat{U} = e^{i\hat{\theta}\hat{S}_y}$  changes the hamiltonian to

$$\hat{\mathcal{H}}'_{\text{lib}} = \frac{(\hat{p}_{\theta} - \hbar\hat{S}_y)^2}{2I} + \frac{1}{2}I\omega_{\theta}^2(\hat{\theta} - \theta')^2 + \hbar D\hat{S}_z^2 + \hbar\gamma_e B(\cos\hat{\theta}\hat{S}_z - \sin\hat{\theta}\hat{S}_x) \quad (10)$$

318 In this frame, the angular momentum  $\hat{p}_{\theta}$  is changed to  $\hat{p}_{\theta} + \hbar\hat{S}_y$ , which is the total  
319 angular momentum of the spin-mechanical system along the  $y$  axis which includes the  
320 librational and the NV-spin angular momentum.

321 Evidently, the correction  $\hbar\hat{S}_y$  will be negligible for a particle with a large inertia. In  
322 order to estimate the relevance of this term in current experiments, one can note that  
323  $\langle\hat{p}_{\theta}\rangle$  is around  $\sqrt{Ik_B T}$  which is far above  $\hbar$  for micron-sized particles (je ne sais pas si  
324 c'est pertinent de comparer en introduisant la température surtout si on veut refroidir,  
325 peut-être faut-il comparer à l'énergie après avoir refroidi qui est  $\hbar\omega_{\theta}$ )

326 Neglecting the contribution from the angular spin momenta, the Hamiltonian reads

$$\hat{\mathcal{H}}'_{\text{lib}} \simeq \frac{\hat{p}_{\theta}^2}{2I} + \frac{1}{2}I\omega_{\theta}^2(\hat{\theta} - \theta')^2 + \hbar D\hat{S}_z^2 + \hbar\gamma_e B \cos\hat{\theta}\hat{S}_z - \hbar\gamma_e B \sin\hat{\theta}\hat{S}_x \quad (11)$$

327 The spin-librational coupling appears clearly in the Zeeman term in this frame.  
328 However, this could be interesting to diagonalize the spin part of the Hamiltonian in  
329 order to see the spin-librational coupling with the NV spin eigenstates. To do so, we  
330 make the small magnetic field assumption  $\gamma_e B \ll D$  and the hypothesis of small mixing  
331 between the two NV excited states characterized by the  $\sin(\theta')^2 \ll \cos(\theta')$  condition.  
332 We also redefine the angle operator  $\hat{\theta}$  around the equilibrium position  $\theta'$ . Under those  
333 assumptions, the Hamiltonian reads (See Appendix A for the detailed calculation):

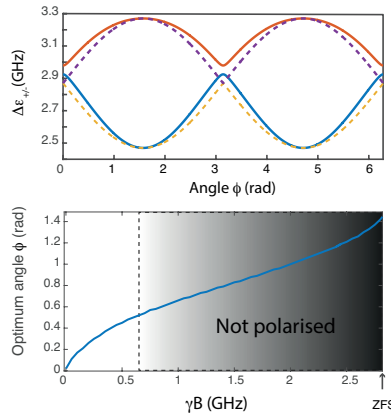
$$\hat{\mathcal{H}}'''_{\text{lib}} \simeq \frac{\hat{p}_{\theta}^2}{2I} + \frac{1}{2}I\omega_{\theta}^2\hat{\theta}^2 + \hbar\omega_{+1}(\hat{\theta})|+1'\rangle\langle+1'| + \hbar\omega_0(\hat{\theta})|0'\rangle\langle0'| + \hbar\omega_{-1}(\hat{\theta})|-1'\rangle\langle-1'| \quad (12)$$

334 where the eigenstates are listed in Appendix XX.  $\omega_i(\hat{\theta}) = \omega_i + \beta_i\hat{\theta}$ .  $\omega_i$  and  $\beta_i$  are  
335 respectively the energies of the eigenstates and the spin-librational coupling constants  
336 calculated in equation (\*) in Appendix A.

<sup>337</sup> In this frame and under the semi-classical approximation for the libration, the  
<sup>338</sup> torque applied on the diamond reads

$$\tau_s = - \left\langle \frac{\partial \hat{H}_{\text{lib}}'''}{\partial \theta} \right\rangle = -\hbar \beta_{+1} \rho_{1',1'} - \hbar \beta_0 \rho_{0',0'} - \hbar \beta_{-1} \rho_{-1',-1'} \quad (13)$$

<sup>339</sup> The eigenstate energies of the spin are represented as a function of  $\theta$  in Fig 1 (mettre  
<sup>340</sup> le plot des énergies des états propres en fonction de l'angle à côté des énergies des états  
<sup>341</sup> propres en fonction du com). Due to the mixing with the excited states, the ground  
<sup>342</sup> state  $|0'\rangle$  acquires a magnetization which is responsible for effects as the Van Vleck  
<sup>343</sup> paramagnetism.



PLOT MAXIME  
 beta\_1,2  
 versus champ mag

**Figure 7.** a) Change in the NV transitions energies as a function of the angle. b) Optimum angle.  
 c) et d)  $\beta_{1,2}$  coefficients.

<sup>344</sup> A question that has to be asked is how the optical pumping process of the NV spin  
<sup>345</sup> is modified by the small mixing between the NV eigenstates in a presence of a transverse  
<sup>346</sup> magnetic field. We show in Appendix B that the pumping process is not modified on  
<sup>347</sup> first order in the transverse magnetic field. As the effects we are looking for are on first  
<sup>348</sup> order, we can neglect the mixing contribution on the optical pumping process of the NV.

## <sup>349</sup> 6. Resonant spin-mechanical interaction: bistability and spin-spring effect

<sup>350</sup> Even if non resonant effects of the spin-librational coupling has recently been  
<sup>351</sup> observed [cite us], adding a micro-wave will make the mechanics and the spin resonantly  
<sup>352</sup> talk to each other. An shift of the equilibrium position for the libration as well as a spin-  
<sup>353</sup> spring effect have been observed.

### <sup>354</sup> 6.1. Resonant spin-mechanical interaction for the center of mass

#### <sup>355</sup> 6.1.1. Hamiltonian calculation

<sup>356</sup> The spin part of the hamiltonian reads

$$\hat{H}_{\text{NV}+\mu\omega} = \hbar D \hat{S}_z^2 + \hbar \gamma_e B_0 \hat{S}_z + \hbar \gamma_e \frac{\partial B_z}{\partial z} z \hat{S}_z + \hbar \Omega \cos(\omega t) \hat{S}_x \quad (14)$$

<sup>357</sup> Moving to the rotating frame of the the microwave frequency with the unitary  
<sup>358</sup> transform  $\hat{U} = e^{i\omega t \hat{S}_z^2}$ , we get under the rotating wave approximation

$$\hat{H}'_{\text{NV}+\mu\omega} = \hbar(D - \omega) \hat{S}_z^2 + \hbar \gamma_e B_0 \hat{S}_z + \hbar \gamma_e \frac{\partial B_z}{\partial z} z \hat{S}_z + \hbar \frac{\Omega}{2} \hat{S}_x \quad (15)$$

<sup>359</sup> We will show that the interplay between a microwave and the Zeeman term can  
<sup>360</sup> lead to a restoring force. Supposing that the micro-wave is close to resonance to the  $|+1\rangle$   
<sup>361</sup> state, we can only consider the  $|0\rangle$  to  $|+1\rangle$  transition neglecting the energy shifts from  
<sup>362</sup> the  $| -1 \rangle$  transition. The two-level system Hamiltonian reads

$$\hat{\mathcal{H}}''_{\text{NV}+\mu\text{w}} = \hbar\Delta(z)|1\rangle\langle 1| + \hbar\frac{\Omega}{2}(|1\rangle\langle 0| + |0\rangle\langle 1|) \quad (16)$$

<sup>363</sup> where  $\Delta(z) = \Delta + \gamma_e \frac{\partial B_z}{\partial z} z$  and  $\Delta = D + \gamma_e B_0 - \omega$ .  
<sup>364</sup> The eigenstates of this hamiltonian are

$$|+\rangle = \cos \Psi |0\rangle + \sin \Psi |1\rangle \quad (17)$$

$$|-\rangle = \sin \Psi |0\rangle - \cos \Psi |1\rangle \quad (18)$$

<sup>365</sup> where

$$\tan 2\Psi = -\frac{\Omega}{\Delta(z)}, \Psi \in [0, \pi/2]. \quad (19)$$

<sup>366</sup> The energies  $E_{\pm} = \hbar/2(\Delta \pm \sqrt{\Delta^2 + \Omega^2})$  of the eigenstate  $|+/-\rangle$  of  $\hat{\mathcal{H}}_{\text{NV}}$  are plotted  
<sup>367</sup> in Fig. 8, for two different values of  $\gamma_e \frac{\partial B_z}{\partial z} z / \Omega$  as a function of  $\Delta/\Omega$ .

<sup>368</sup> Let us consider positive detuning  $\Delta$  and a mixing angle  $\Psi$  close to  $\pi/2$ , where the  
<sup>369</sup> states  $|0\rangle$  and  $|1\rangle$  are only slightly perturbed by the microwave tone. In this so-called  
<sup>370</sup> dispersive limit, the eigenstates of  $\hat{\mathcal{H}}''_{\text{NV}+\mu\text{w}}$  are close to being those of  $\hat{S}_z$ . Note that, due  
<sup>371</sup> to the intersystem crossing in the optically excited state of the NV center, the state that  
<sup>372</sup> is populated in the steady state is the state with the largest projection onto the bare  $|0\rangle$   
<sup>373</sup> state and the population will always remain there if the position rate of change is slow  
<sup>374</sup> compared to the typical splittings. The NV centers electronic spins are thus mostly in  
<sup>375</sup> the ground state  $|-\rangle$  when  $\Delta > 0$ . As can be seen in Fig. 8, the magnetic energy thus  
<sup>376</sup> increases when  $z$  increases, so the electronic spins exert a restoring force which tends to  
<sup>377</sup> bring back the particle at the  $z = 0$  position.

### <sup>378</sup> 6.1.2. Static phenomena: bistability

<sup>379</sup> Formally, the spin-force operator reads

$$\hat{F}_s = -\frac{\partial \hat{\mathcal{H}}''_{\text{NV}+\mu\text{w}}}{\partial z} = -\hbar G_z |1\rangle\langle 1| \quad (20)$$

<sup>380</sup> where  $G_z = \gamma_e \frac{\partial B_z}{\partial z}$ . In the state  $|-\rangle$ , we get

$$\langle -|\hat{F}|-\rangle = -\hbar G_z |\langle -|1\rangle|^2 \approx -\hbar G_z \left( \frac{\Omega}{\Delta(z)} \right)^2 \quad (21)$$

<sup>381</sup> Depending on the intensity of the microwave power and the detuning  $\Delta$ , this spin  
<sup>382</sup> potential combined with the trapping angular mechanism will allow one or two stable  
<sup>383</sup> positions.

<sup>384</sup> The new angular stable position is given by the equation:

$$F_s + F_{\text{trapping}} = 0 \quad (22)$$

<sup>385</sup> which gives rise to a third degree polynomial equation:

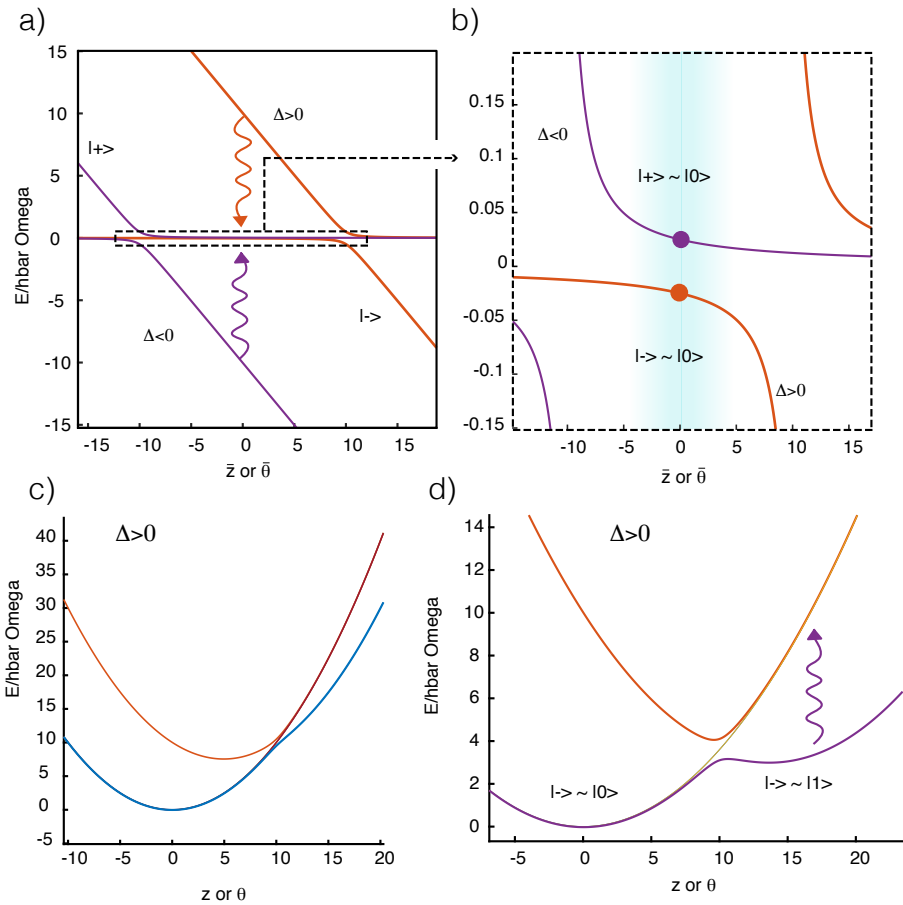


**Figure 8.** a) Energies of the two dressed eigenstates for the  $|0\rangle$  to  $|+1\rangle$  spin transition as a function of the rescaled position and angle  $z$  or  $\theta$ .  $\bar{z} = (\gamma_e \frac{\partial B}{\partial z} / \Omega)z$  for the  $z$ -position and  $\bar{\theta} = (\gamma_e B / \Omega)\theta$  for the angular degree of freedom. Red (resp. blue) line: the detuning was increased (resp. decreased) by  $\Delta/\Omega = 10$ . Red and blue curly arrows depict transitions between dressed states mediated by the laser. b): zoom on the dashed rectangle in a). The blue shaded area indicates the regime where the regime where the magnetic energy in the  $|\pm\rangle$  states can be added to the free mechanical energy. c) and d) Mechanical energy and magnetic energy as a function of the rescaled position and angles. NUMBERS TO COME.

$$\hbar G_z \Omega^2 + m\omega_z^2 z(\Delta + G_z z)^2 = 0 \quad (23)$$

386 The bistability in the equilibrium position occurs when the coupling is strong  
 387 enough and  $\Delta < 0$ . We can note  $z_0$  this new equilibrium position.

388 6.1.3. Dynamical backaction: spin-spring effect

389 Linearizing about the new equilibrium position  $z_0$  and introducing  $\bar{\Delta} = \Delta + G_z z_0$   
 390 the apparent detuning at the new equilibrium position, we get

$$\langle -|\hat{F}_s|-\rangle \approx F_{s,0} + K_s(z - z_0) \quad (24)$$

391 where

$$F_{s,0} = \hbar G_z \left( \frac{\Omega}{\bar{\Delta}} \right)^2 \quad (25)$$

<sup>392</sup> and

$$K_s = -2\hbar G_z^2 \frac{\Omega^2}{\bar{\Delta}^3} \quad (26)$$

<sup>393</sup> in the limit of small angle shifts.

<sup>394</sup> We thus have a restoring force in the limit where  $\bar{\Delta} > 0$  (blue detuned with respect  
<sup>395</sup> to the spin transition) as anticipated.

<sup>396</sup> The strength of the shift must be compared to the restoring force from the bare  
<sup>397</sup> mechanical oscillator. Further, in the presence of laser light, transitions from the dressed  
<sup>398</sup> state tend to alter this predicted shift.

#### <sup>399</sup> 6.1.4. Hamiltonian calculation

<sup>400</sup> In this part, we will obtain a simplified spin-mechanical Hamiltonian for the libra-  
<sup>401</sup> tion in a presence of a micro-wave. The total Hamiltonian reads in the lab frame:

$$\hat{\mathcal{H}}_{\text{NV+}\mu\text{w}} = \hbar D \hat{S}_z^2 + \hbar \gamma_e B \hat{S}_z + \hbar \Omega \cos(\omega t) \hat{S}_x \quad (27)$$

<sup>402</sup> where  $\Omega$  is the micro-wave power and  $\omega$  the micro-wave frequency. We can now  
<sup>403</sup> simplify this Hamiltonian by doing the same unitary transforms than before without the  
<sup>404</sup> micro-wave. Furthermore, we can move to the rotating frame of the micro-wave doing  
<sup>405</sup> the time-depending transform  $\hat{U}' = e^{i\omega t \hat{S}_z^2}$  and under the rotating-wave approximation,  
<sup>406</sup> we obtain the Hamiltonian by redefining  $\Omega \equiv \Omega \cos(\theta')$  (calculation are presented in  
<sup>407</sup> Appendix A):

$$\hat{\mathcal{H}}'_{\text{NV+}\mu\text{w}} \simeq \hbar \Delta_{+1}(\hat{\theta}) |+1'\rangle \langle +1'| + \hbar \Delta_0(\hat{\theta}) |0'\rangle \langle 0'| + \hbar \Delta_{-1}(\hat{\theta}) |-1'\rangle \langle -1'| + \hbar \frac{\Omega}{2} \hat{S}_x \quad (28)$$

<sup>408</sup> where  $\Delta_{+1}(\hat{\theta}) = \omega_{+1}(\hat{\theta}) - \omega$ ,  $\Delta_{-1}(\hat{\theta}) = \omega_{-1}(\hat{\theta}) - \omega$  and  $\Delta_0(\hat{\theta}) = \omega_0(\hat{\theta})$ .

<sup>409</sup> The eigenstates are listed in Appendix XX.

<sup>410</sup> Supposing that the micro-wave is close to resonance with the upper eigenstate  
<sup>411</sup>  $|1'\rangle$  transition of the NV center, we can then neglect the influence of the  $|-1'\rangle$  state  
<sup>412</sup> and then reduce the study to a two dimensional Hilbert space. Note that the optical  
<sup>413</sup> pumping process is stronger than the relaxation rate  $T_1$  between the states and so we  
<sup>414</sup> can reasonably consider that  $\rho_{-1',-1'} \ll 1$ . This justifies that the whole study of this  
<sup>415</sup> Hamiltonian including the dissipation process can be reduced to this two-level system.

$$\hat{\mathcal{H}}''_{\text{NV+}\mu\text{w}} \simeq \hbar (\Delta + (\beta_1 - \beta_0)\hat{\theta}) |1'\rangle \langle 1'| + \hbar \beta_0 \hat{\theta} \hat{I}d + \hbar \frac{\Omega}{2} (|0\rangle \langle 1'| + |1'\rangle \langle 0|) \quad (29)$$

<sup>416</sup> where  $\Delta = \Delta_1 - \Delta_0$  and  $\Omega \equiv \frac{\Omega}{\sqrt{2}}$  to take into account  $\sqrt{2}$  of the Spin 1  $\hat{S}_x$  operator.

<sup>417</sup> We have fixed the energy reference in the  $|0'\rangle$  state. The second term operates as a small  
<sup>418</sup> shift of the angular position and can be interpreted as the Van Vleck paramagnetism. We  
<sup>419</sup> can then redefine our mechanical resonator around this equilibrium position which is  
<sup>420</sup> the one taken by the mechanical oscillator when all the population is in the  $|0'\rangle$  state. It  
<sup>421</sup> corresponds to the equilibrium position in the experiment because the  $|0'\rangle$  is populated  
<sup>422</sup> with a continuous green laser. We include in  $\Delta$  the shift of  $\hat{\theta}$  in the first term of the  
<sup>423</sup> Hamiltonian. Furthermore, by defining  $G_0 = \beta_1 - \beta_0$  the spin-mechanical constant for

<sup>424</sup> one spin and treating classically the angle, the Hamiltonian of the system can finally be  
<sup>425</sup> written as a simple two-level atom model:

$$\hat{\mathcal{H}}''_{\text{NV}+\mu w} = \begin{pmatrix} \Delta(\theta) & \Omega/2 \\ \Omega/2 & 0 \end{pmatrix} \quad (30)$$

<sup>426</sup> where  $\Delta(\theta) = \Delta + G_0\theta$  is the frequency difference between the ground and excited state  
<sup>427</sup> 1.

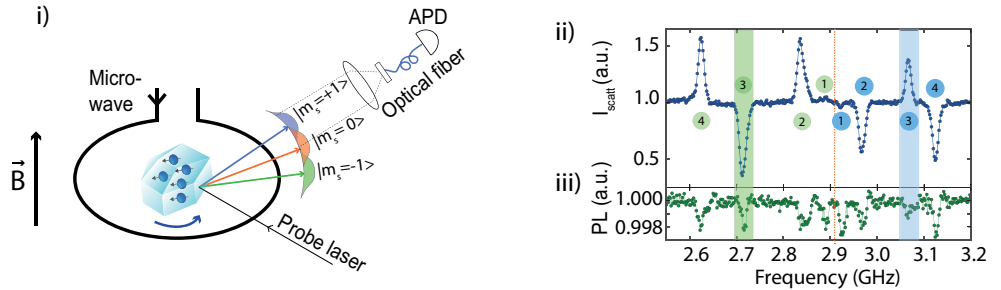


**Figure 9.** Spin torque

#### <sup>428</sup> 6.1.5. Static phenomena: bistability

<sup>429</sup> One of the important first order effect that can be observed in the spin part of the  
<sup>430</sup> hamiltonian is a shift in the excited state population when the microwave is detuned  
<sup>431</sup> with respect to the transition. Further, due to the angular dependence of the energy of  
<sup>432</sup> the excited state, the shift here depends on the angle of the particle (as it does for the  
<sup>433</sup> position in the presence of a magnetic field gradient). This then also implies a shift in  
<sup>434</sup> the librational frequency. The shift in the energy is shown in Fig. 8 for  $\Delta > 0$ . The angle  
<sup>435</sup> is reduced when going from the dashed energy lines to the plain lines in this example.  
<sup>436</sup> In the ground state, the corresponding energy decreases, we thus expect an anti-binding  
<sup>437</sup> torque in this regime. Similar to above, the torque  $\tau_s(\theta)$  exerted on the particle in the  
<sup>438</sup> state  $|1'\rangle$  can then be evaluated to be

$$\hat{\tau}_s = -\frac{\partial \hat{\mathcal{H}}''_{\text{NV}+\mu w}}{\partial \theta} = -\hbar G_0 |1'\rangle \langle 1'| \quad (31)$$

<sup>439</sup> In the dispersive limit where  $\Omega \ll \Delta(\theta)$ , we are mostly in the  $|-\rangle$  state and the  
<sup>440</sup> torque is equal to:

$$\tau_s = \langle -|\hat{\tau}_s|-\rangle = -\hbar G_0 |\langle -|1'\rangle|^2 \approx -\hbar G_0 \left( \frac{\Omega}{\Delta(\theta)} \right)^2 \quad (32)$$

<sup>441</sup> Depending on the intensity of the microwave power and the detuning  $\Delta$ , this spin  
<sup>442</sup> torque combined with the trapping angular mechanism will allow one or two stable  
<sup>443</sup> positions.

<sup>444</sup> The new angular stable position is given by the equation:

$$\tau_s + \tau_{\text{trapping}} = 0 \quad (33)$$

<sup>445</sup> which gives rise to a third degree polynomial equation:

$$\hbar G_0 \Omega^2 + I \omega_\theta^2 \theta (\Delta + G_0 \theta)^2 = 0 \quad (34)$$

<sup>446</sup> The bistability in the equilibrium position occurs when the coupling is strong  
<sup>447</sup> enough and  $\Delta < 0$ . We can note  $\theta_0$  this new equilibrium position.

#### <sup>448</sup> 6.1.6. Dynamical backaction: spin-spring effect

<sup>449</sup> Linearizing about the new equilibrium position  $\theta_0$  and introducing  $\bar{\Delta} = \Delta + G_0\theta_0$   
<sup>450</sup> the apparent detuning at  $\theta_0$ , we get

$$\langle -|\hat{\tau}_s|-\rangle \approx \tau_{s,0} + K_s(\theta - \theta_0) \quad (35)$$

<sup>451</sup> where

$$\tau_{s,0} = \hbar G_0 \left( \frac{\Omega}{\bar{\Delta}} \right)^2 \quad (36)$$

<sup>452</sup> and

$$K_s = -2\hbar G_0^2 \frac{\Omega^2}{\bar{\Delta}^3} \quad (37)$$

<sup>453</sup> in the limit of small angle shifts.

<sup>454</sup> We thus have a restoring torque in the limit where  $\bar{\Delta} > 0$  (blue detuned with respect  
<sup>455</sup> to the spin transition) as anticipated.

<sup>456</sup> The strength of the shift must be compared to the restoring force from the bare  
<sup>457</sup> mechanical oscillator. Further, in the presence of laser light, transitions from the dressed  
<sup>458</sup> state tend to alter this predicted shift.

## <sup>459</sup> 7. Resonant spin-mechanical interaction: spin-cooling

<sup>460</sup> In order to evaluate the dynamical backaction from the spins to the mechanical  
<sup>461</sup> oscillator, one needs to include the full dynamics plus the dissipation. Only the libration  
<sup>462</sup> treatment will be performed but the equation of motion are the same for the CoM.

### <sup>463</sup> 7.1. Equations of motion

<sup>464</sup> For a small longitudinal decay  $T_1$  compared to the optical pumping process of the  
<sup>465</sup> NV center, the magnetic state  $| -1' \rangle$  is not populated. We can thus reduce the study to  
<sup>466</sup> the two level system Hamiltonian obtained in equation (\*).

Using the von Neumann equation, we obtain

$$\frac{\partial \rho_{10}}{\partial t} = (-\Gamma_2^* + i\Delta(\theta))\rho_{10} + i\frac{\Omega}{2}(2\rho_{11} - 1) \quad (38)$$

$$\frac{\partial \rho_{11}}{\partial t} = -\gamma_{\text{las}}\rho_{11} + i\frac{\Omega}{2}(\rho_{10} - \rho_{10}^*) \quad (39)$$

<sup>467</sup> where  $\Gamma_2^*$  is the inhomogeneous broadening of the NV center and  $\gamma_{\text{las}}$  is the optical  
<sup>468</sup> pumping rate in the  $| 0' \rangle$  state.

<sup>469</sup> This equation is coupled to the equation of motion of the particle

$$I \frac{\partial^2 \theta}{\partial t^2} + I\gamma \frac{\partial \theta}{\partial t} + I\omega_\theta^2 \theta = \langle \hat{\tau}_s \rangle + \tau_L \quad (40)$$

<sup>470</sup> where  $\langle \hat{\tau}_s \rangle = -\hbar G_0 \rho_{11}$ .

<sup>471</sup> This system of equation is nonlinear given the dependancy in  $\theta$  of the detuning  
<sup>472</sup> in equation (36). A usual treatment that has been performed in optomechanics is to  
<sup>473</sup> study the system dynamic around a steady-state by linearizing the set of equations. This  
<sup>474</sup> approach will be performed on our set of equation.

**475** 7.1.1. Stationary solutions

**476** We introduce the steady-state quantities as  $\rho_{1,1}^0 = \langle \rho_{1,1} \rangle$ ,  $\rho_{1,0}^0 = \langle \rho_{1,0} \rangle$  and  $\theta_0 = \langle \theta \rangle$ .  
**477** Writing the shifted detuning  $\bar{\Delta} = \Delta(\theta_0)$  and the incoherent pumping rate to the magnetic  
**478** state  $\Gamma_0 = \frac{\Omega^2 \Gamma_2^*}{\Gamma_2^{*2} + \bar{\Delta}^2}$ , we get:

$$\rho_{11}^0 = \frac{1}{2} \frac{\Gamma_0}{\gamma_{\text{las}} + \Gamma_0} \quad (41)$$

**479** Using the equation of motion for the angle, we obtain:

$$I\omega_\theta^2 \theta_0 = \langle \hat{\tau}_s \rangle = -\hbar G_0 \rho_{11}^0 \quad (42)$$

**480** This last equation gives us a third degree polynomial equation for  $\theta_0$ . Depending  
**481** on the microwave detuning, there are either one or two stable solutions for  $\theta_0$ .

**482** 7.1.2. Effective susceptibility

We want to study the dynamic of the system in a linear regime. Writing each quantity as  $f(t) = \langle f \rangle + \delta f(t)$  and by looking at the dynamical equation in the Fourier space, we get

$$\delta\theta(\omega) = \chi_{\text{eff}}(\omega) \delta\tau_L(\omega)$$

**483** where

$$\chi_{\text{eff}}(\omega) = \frac{1}{I(\omega_\theta^2 - \omega^2 - i\omega\gamma) - K(\omega)} \quad (43)$$

**484** The quantity  $K(\omega)$  is a dynamical spin-stiffness. The real part of  $K(\omega)$  gives rise to an  
**485** increase or decrease of the mechanical oscillator frequency while the imaginary part acts  
**486** as a cooling or a heating of the mechanical motion. We can rewrite the susceptibility in a  
**487** condensed form

$$\chi_{\text{eff}}(\omega) = \frac{1}{I(\tilde{\omega}_\theta^2 - \omega^2 - i\omega\tilde{\gamma})} \quad (44)$$

**488** with

$$\tilde{\omega}_\theta = \omega_\theta [1 - \frac{\text{Re}(K(\omega_\theta))}{2K_t}] \quad \text{and} \quad \tilde{\gamma} = \gamma [1 + Q \frac{\text{Im}(K(\omega_\theta))}{K_t}] \quad (45)$$

**489** the modified damping and frequency of the mechanical oscillator in the limit  $\omega_\theta \gg$   
**490**  $\text{Re}(K(\omega_\theta))/K_t$ . Here  $K_t = I\omega_\theta^2$  is the trap stiffness and  $Q = \omega_\theta/\gamma$  is the trap quality  
**491** factor. In the modified shifts and damping formulae, we suppose  $\omega = \omega_\theta$ .

**492** The spin-mechanical damping originates from the delay between the NV center  
**493** acquired magnetization and the Paul trap restoring torque.

**494** 7.1.3. Time-dependent solutions

**495** In the adiabatic limit where  $\omega_\theta \ll \Delta$ , we can consider  $\frac{\partial \rho_{10}}{\partial t} \approx 0$  and by injecting the  
**496** equation for the coherence into the equation of population we get

$$\frac{\partial \rho_{11}}{\partial t} = -\gamma_{\text{las}} \rho_{11} - \frac{\Omega^2}{2\Gamma_2^*} \mathcal{L}(\theta) (2\rho_{11} - 1) \quad (46)$$

**497** where

$$\mathcal{L}(\theta) = \frac{1}{1 + (\Delta(\theta)/\Gamma_2^*)^2} \quad (47)$$

<sup>498</sup> We now linearize equation (\*) around the steady states and move to the Fourier  
<sup>499</sup> space. We find:

$$K(\omega) = \hbar \bar{\Delta} \frac{(\alpha\tau)^2}{1 + i\omega\tau}, \quad (48)$$

where

$$\alpha = G_0 \sqrt{\frac{\gamma_{\text{las}} \Gamma_0^2}{\Gamma_2^* \Omega^2}} \quad \text{and} \quad \tau = (\gamma_{\text{las}} + \Gamma_0)^{-1}.$$

<sup>500</sup> Finally, we can determine the modified frequency and damping of the libration  
<sup>501</sup> using equation (\*)

$$\tilde{\omega}_\theta = \omega_\theta [1 + \frac{\hbar}{2K_t} \frac{(\alpha\tau)^2}{1 + (\omega_\theta\tau)^2} \bar{\Delta}] \quad (49)$$

<sup>502</sup> and

$$\tilde{\gamma} = \gamma [1 - Q \frac{\hbar(\alpha\tau)^2(\omega_\theta\tau)}{K_t(1 + (\omega_\theta\tau)^2)} \bar{\Delta}] \quad (50)$$

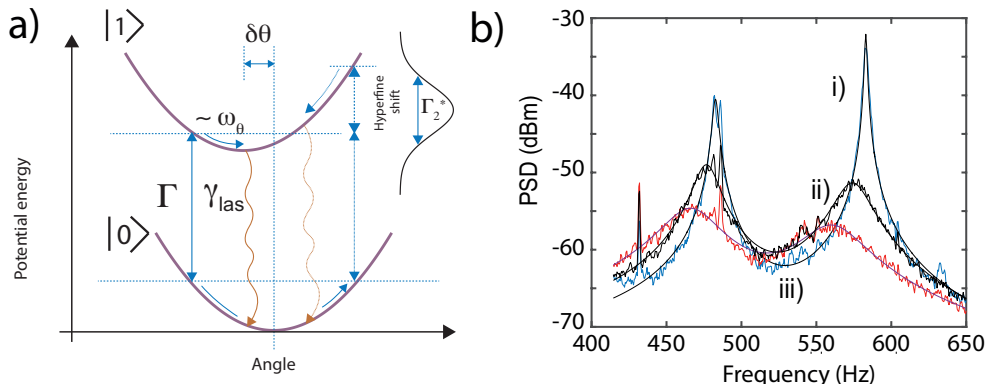


**Figure 10.** Spin-cooling in the adiabatic limit

## <sup>503</sup> 8. Sensing

<sup>504</sup> In this chapter, we discuss the various possibilities offered by NV centers coupled to  
<sup>505</sup> levitating mechanical oscillators in terms of sensors. In the first part, we discuss sensors  
<sup>506</sup> based on motional detection. We conclude by presenting the sensing of the motion using  
<sup>507</sup> photoluminescence detection from NVs.

<sup>508</sup> The schemes we have in mind are : A levitating diamonds with embedded NVs or  
<sup>509</sup> a levitating magnet coupled to an NV center.

### <sup>510</sup> 8.1. Sensing based on motional detection

<sup>511</sup> Here, the calculation is relevant to the experiment performed in DELORD, where  
<sup>512</sup> the NVs could move a levitating diamond. The main ideas are similar to MRFM though.

<sup>513</sup> The noise is supposed to be largely due to the Brownian motion of the levitating  
<sup>514</sup> object.

#### <sup>515</sup> 8.1.1. Force or torque sensing using mechanical oscillators

<sup>516</sup> BOWEN

<sup>517</sup> In this part, no information about the specific force or torque is needed. The concepts  
<sup>518</sup> are general to any oscillator driven by brownian motion. Let us consider that the torque  
<sup>519</sup> signal one wishes to measure is modulated at a mechanical response.

<sup>520</sup> We write

$$\Gamma_s(t) = \Gamma_s \cos(\omega_\theta t). \quad (51)$$

<sup>521</sup> We also have

$$I\ddot{\theta} + I\gamma\dot{\theta} + I\omega_\theta^2\theta = \Gamma_s(t) + \Gamma_T(t) \quad (52)$$

<sup>522</sup> where  $\Gamma_T(t)$  is the Langevin torque. The librational spectrum reads :

$$S_\theta(\omega) = |\chi(\omega)|^2 [S_T(\omega) + S_{\text{spin}}(\omega)] \quad (53)$$

<sup>523</sup> The fluctuation dissipation theorem at large temperatures gives :

$$S_T(\omega) = 2kT\gamma I \quad (54)$$

<sup>524</sup> in the high temperature limit. We also have

$$S_s(\omega) = \frac{1}{2}\Gamma_s^2(\delta(\omega - \omega_\theta) + \delta(\omega + \omega_\theta)) \quad (55)$$

<sup>525</sup> Integrating  $S_\theta(\omega, \Gamma_s, \gamma = 0)$  and  $S_\theta(\omega, \gamma, \Gamma_s = 0)$  over some detection bandwidth  $b$   
<sup>526</sup> we get a signal

$$S = \frac{1}{2}\Gamma_s^2|\chi(\omega)|^2 \quad (56)$$

<sup>527</sup> and a noise

$$\sigma = 2kT\gamma I|\chi(\omega)|^2 b \quad (57)$$

<sup>528</sup> The minimum torque  $\Gamma_s^{\min}$  that can be detected is obtained by setting  $S = \sigma$ . The  
<sup>529</sup> signal to noise is then unity, which defines  $\Gamma_s^{\min}$  to be

$$\Gamma_s^{\min} = \sqrt{4kT\gamma Ib} = \sqrt{\frac{4kTK_t b}{Q\omega_\theta}} \quad (58)$$

<sup>530</sup> where  $Q = \omega_\theta/\gamma$  is the quality factor of the mechanical oscillator, and  $K_t$  is the trap  
<sup>531</sup> stiffness, namely  $I\omega_\theta^2$ .

<sup>532</sup> The largest sensitivities with levitating systems have been achieved using levitating  
<sup>533</sup> silica nanospheres. GERACI and TONGCANG  $10^{-28}$  N.m/ $\sqrt{\text{Hz}}$ .

<sup>534</sup> With larger particles, a sensitivity of  $10^{-23}$  N.m/ $\sqrt{\text{Hz}}$  was attained in HUILLYERY  
<sup>535</sup> at only  $10^{-2}$  mbars. Remarkably, these sensitivities are very close to the state of the art  
<sup>536</sup> torque sensing obtained at dilution fridge temperatures. Highlighting the powerfullness  
<sup>537</sup> of levitating platforms.

<sup>538</sup> Systems that use an internal degree of freedom show a little lower performance due  
<sup>539</sup> to the constraints mentioned in chap 1 related to the vacuum conditions as well as the  
<sup>540</sup> required large particle size for angular stability. Both contribute to lowering this figure.

<sup>541</sup> Of course this limit does not include a detailed analysis of the signal that one must  
<sup>542</sup> acquire to probe the oscillator. The frequency of the mechanical oscillator must be  
<sup>543</sup> well defined over the course of the measurement. Far from equilibrium situations may  
<sup>544</sup> actually enable the frequency to be measured, but the sensitivity will be greatly reduced

<sup>545</sup> if the particle regularly spins for instance or if it is excited by extra forces. A careful check  
<sup>546</sup> of the noise sources and the thermal equilibrium with the surrounding gas temperature  
<sup>547</sup> must be used before employing this formula. Note that cooling the mechanical oscillator  
<sup>548</sup> via cold damping will not help since  $T \times \gamma$  will be constant.

#### <sup>549</sup> 8.1.2. Magnetic field sensing

<sup>550</sup> Levitating particles that contain nitrogen vacancy centers may also be employed  
<sup>551</sup> for performing magnetometry.

<sup>552</sup> The idea is depicted in Fig. 1.

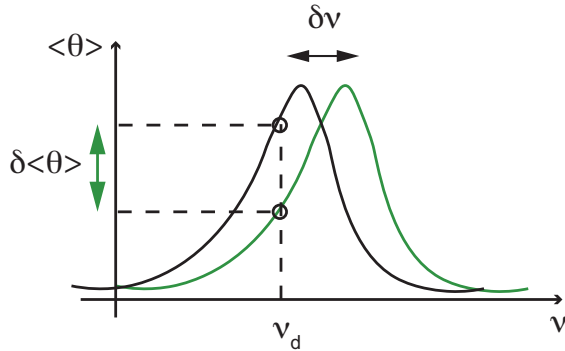


**Figure 11.** ESR

<sup>553</sup> The idea of the magnetometer is similar to NV magnetometry : an external B field  
<sup>554</sup> lifts the degeneracy between the states  $\pm 1$ . Here however a laser detects the rotation  
<sup>555</sup> of the particle when a microwave hits an ESR. The main difference from ODMR is the  
<sup>556</sup> response with respect to the B field. In ODMR, under strong B fields, mixing from small  
<sup>557</sup> angles can blur the signal. Here, a bias  $B_0$  field would be needed in order to get a strong  
<sup>558</sup> torque.

<sup>559</sup> Here a change in the B field induces a change in the magnetization  $S_z$  in the presence  
<sup>560</sup> of a detuned microwave, which rotates the particle, hence changing the count-rate. We  
<sup>561</sup> assume a single NV center and neglect the effects of B field mixing on the eigenstates.

<sup>562</sup> The change of the magnetic field changes the spin torque  $\Gamma_s$  via a change in the  
<sup>563</sup> population in the magnetic state via

$$\delta\Gamma_s = \hbar N \gamma B_0 \delta\rho_m(t) \quad (59)$$

<sup>564</sup> for instance.

<sup>565</sup>  $\rho_m$  is the density matrix diagonal term component for the  $-1$  or  $+1$  state respec-  
<sup>566</sup> tively.

$$\delta\Gamma_s = \hbar N \gamma B_0 \frac{\partial \rho_m(t)}{\partial B} \delta B(t) \quad (60)$$

<sup>567</sup> We thus get

$$\delta B_{\min} = \frac{\delta\Gamma_s^{\min}}{\hbar N \gamma B_0 \frac{\partial \rho_m(t)}{\partial B}} \quad (61)$$

<sup>568</sup> We now estimate the change in the population in the excited spin state changes  
<sup>569</sup> when B changes. This takes place because of the change in the detuning, hence of the  
<sup>570</sup> microwave excitation efficiency. We write C the ESR contrast, which depends on the  
<sup>571</sup> various parameters of the intersystem crossing. It can be about 20 %.

We have :

$$\rho_m = \frac{C\Gamma^2}{(\Gamma_2^*)^2 + (\Delta + \gamma_e B\theta)^2 + 2\Gamma^2} \approx \frac{C\Gamma^2}{(\Gamma_2^*)^2 + 2\Gamma^2 + \Delta^2}$$

<sup>572</sup> with  $\Gamma = 2\Omega^2\Gamma_2^*/(\Gamma_1 + \gamma_{\text{las}})$ .  $\Omega$  is the microwave Rabi frequency,  $\Gamma_1$  the longitudinal  
<sup>573</sup> decay rate and  $\Delta$  is the microwave detuning. In this approximate equation, we neglected  
<sup>574</sup> the non-linear effects as well as the cooling/heating effects. This comes down to neglecting  
<sup>575</sup> back-action on the spin state when the diamond turns; namely the term  $\gamma_e B\theta$  in the  
<sup>576</sup> equation for  $\rho_m$ .

Importantly, the microwave detuning  $\Delta \approx \omega - (D - \gamma_e B)$  depends on the B field as in ODMR based magnetometry.

$$\frac{\partial \rho_m}{\partial B} = \gamma_e \frac{\partial \rho_m}{\partial \Delta} = -2C\gamma_e \frac{\Gamma^2 \Delta}{((\Gamma_2^*)^2 + \Gamma^2 + \Delta^2)^2}$$

To have the best sensitivity, one parks oneself to  $\Delta = -\Gamma_2^*$ . We then get

$$\frac{\partial \rho_m}{\partial B} \approx 2C\gamma_e \frac{\Gamma^2}{(\Gamma_2^*)^3}$$

<sup>577</sup> .  
<sup>578</sup> There is a trade off between excitation efficiency and width. In the pulsed mi-  
<sup>579</sup> crowave excitation regime however, one gets [? ] :

$$\frac{\partial \rho_m}{\partial B} \approx C \frac{\gamma_e}{\Gamma_2^*}$$

<sup>580</sup> Plugging this into the equation for  $\delta B_{\min}$  One finds  $\eta=100$  nT/ $\sqrt{\text{Hz}}$ .

<sup>581</sup> We concentrate on the read-out of a mechanical oscillator, driven or undergoing  
<sup>582</sup> Brownian motion.

### <sup>583</sup> 8.2. Sensing the motion using on photoluminescence detection

<sup>584</sup> The experiments here are Kolkowitz, Huillery, Arcizet, ect.

<sup>585</sup> BENNETT ET AL.

<sup>586</sup> In Gieseler et al. a time dependent magnetic field was used to excite the motion of  
<sup>587</sup> the trapped magnet. The magnetic field oscillation generated by the magnet at the NV  
<sup>588</sup> location was observed as a peak in the power spectral density of the NV count rates.

<sup>589</sup> In Huillery et al. a hybrid particle was trapped...

<sup>590</sup> Similar read-out schemes have been used in tethered platforms in the past.

<sup>591</sup> **Author Contributions:** “Conceptualization, X.X. and Y.Y.; methodology, X.X.; software, X.X.; vali-  
<sup>592</sup> dation, X.X., Y.Y. and Z.Z.; formal analysis, X.X.; investigation, X.X.; resources, X.X.; data curation,  
<sup>593</sup> X.X.; writing—original draft preparation, X.X.; writing—review and editing, X.X.; visualization,  
<sup>594</sup> X.X.; supervision, X.X.; project administration, X.X.; funding acquisition, Y.Y. All authors have  
<sup>595</sup> read and agreed to the published version of the manuscript.”

<sup>596</sup> **Funding:** This research was funded by NAME OF FUNDER grant number XXX.”

<sup>597</sup> **Data Availability Statement:** In this section, please provide details regarding where data sup-  
<sup>598</sup> porting reported results can be found, including links to publicly archived datasets analyzed or  
<sup>599</sup> generated during the study. Please refer to suggested Data Availability Statements in section  
<sup>600</sup> “MDPI Research Data Policies” at <https://www.mdpi.com/ethics>. You might choose to exclude  
<sup>601</sup> this statement if the study did not report any data.

<sup>602</sup> **Acknowledgments:** We would like to acknowledge fruitful discussions with Samuel Deléglise,  
<sup>603</sup> Itsik Cohen, Cosimo Rusconi, Oriol Roméro-Isard and Ben Stickler.

<sup>604</sup> **Conflicts of Interest:** The authors declare no conflict of interest.’

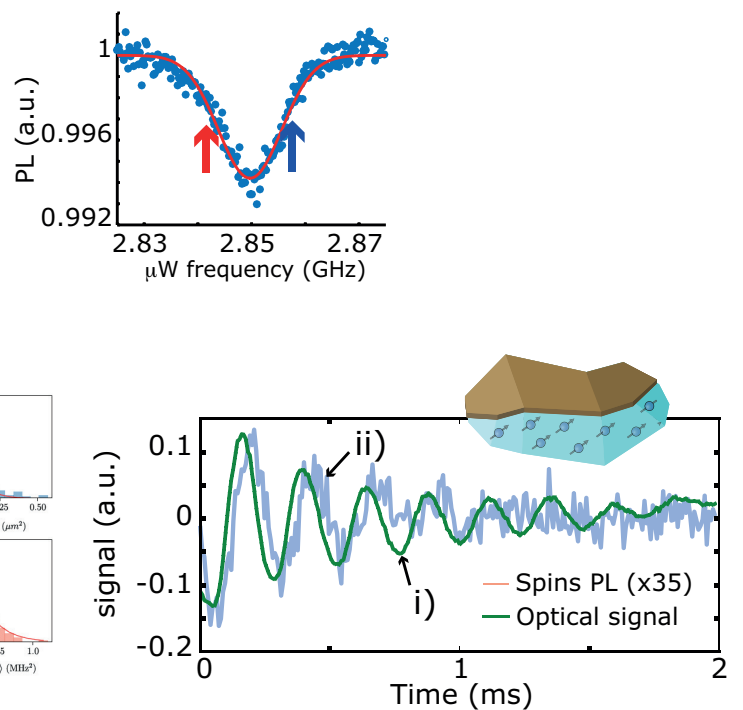


**Figure 12.** Experiments where the PL is used for sensing the motion.

## Abbreviations

- The following abbreviations are used in this manuscript:
- MDPI Multidisciplinary Digital Publishing Institute
  - DOAJ Directory of open access journals
  - TLA Three letter acronym
  - LD Linear dichroism

## Appendix A

### Appendix A.1

The appendix is an optional section that can contain details and data supplemental to the main text—for example, explanations of experimental details that would disrupt the flow of the main text but nonetheless remain crucial to understanding and reproducing the research shown; figures of replicates for experiments of which representative data are shown in the main text can be added here if brief, or as Supplementary Data. Mathematical proofs of results not central to the paper can be added as an appendix.

**Table A1.** This is a table caption. Tables should be placed in the main text near to the first time they are cited.

Title 1	Title 2	Title 3
Entry 1	Data	Data
Entry 2	Data	Data

## Appendix B

All appendix sections must be cited in the main text. In the appendices, Figures, Tables, etc. should be labeled, starting with “A”—e.g., Figure A1, Figure A2, etc.

## 620 Appendix C Derivation of a simplified Hamiltonian

621 In this section we detail the calculation of the simplified spin-libration Hamiltonian  
 622 obtained in equation (\*). Few unitary transformations will be performed on the Hamilto-  
 623 nian. For the sake of simplicity, we will divide our Hamiltonian in three different parts  
 624 to do the calculation and see the effect of each transformation on the different parts :

$$\hat{\mathcal{H}} = \hat{\mathcal{H}}_{\text{mecha}} + \hat{\mathcal{H}}_{\text{NV}} + \hat{\mathcal{H}}_{\mu\text{w}} \quad (\text{A1})$$

625 where

$$\hat{\mathcal{H}}_{\text{mecha}} = \frac{\hat{p}_\theta^2}{2I} + \frac{1}{2} I \omega_\theta^2 (\hat{\theta} - \theta')^2 \quad (\text{A2})$$

$$\hat{\mathcal{H}}_{\text{NV}} = \hbar D \hat{S}_{z'}^2 + \hbar \gamma_e B \hat{S}_z \quad (\text{A3})$$

$$\hat{\mathcal{H}}_{\mu\text{w}} = \hbar \Omega \cos(\omega t) \hat{S}_x \quad (\text{A4})$$

626 Three main approximations are being done to derive this Hamiltonian.

627 Firstly, we suppose the magnetic field intensity  $\gamma_e B$  to be smaller than the anisotropy  
 628 pulsation of the NV center  $D$ . Secondly, we suppose the transverse magnetic field  $B_\perp$   
 629 and the longitudinal magnetic field  $B_\parallel$  to be of the same order of magnitude.

630 Thirdly, we also suppose that the angular momenta of the particle given by the  
 631 mean value  $\langle \hat{p}_\theta \rangle$  is few order of magnitude taller than the typical spin momenta  $\hbar \langle \hat{S}_y \rangle$ .  
 632 This assumption is totally valid for micron-sized particle.

### 633 Appendix C.1 NV center Hamiltonian derivation

634 In this section, we derive the calculation of the NV center Hamiltonian. The initial  
 635 Hamiltonian reads :

$$\hat{\mathcal{H}}_{\text{NV}} = \hbar D \hat{S}_{z'}^2 + \hbar \gamma_e B \hat{S}_z \quad (\text{A5})$$

#### 636 Appendix C.1.1 Moving to the particle frame

637 We can move to the particle frame by doing the unitary transformation  $\hat{U} = e^{i\hat{\theta}\hat{S}_y}$   
 638 which gives the Hamiltonian :

$$\hat{\mathcal{H}}'_{\text{NV}} = \hbar D \hat{S}_z^2 + \hbar \gamma_e B (\cos \hat{\theta} \hat{S}_z - \sin \hat{\theta} \hat{S}_x) \quad (\text{A6})$$

639 In this frame, the eigenstates of the spin operator  $\hat{S}_z$  are the ones where the optical  
 640 pumping process of the green laser takes place.

#### 641 Appendix C.1.2 Moving to the diagonalized basis of the NV Hamiltonian

642 We want to diagonalize the NV part of the Hamiltonian in the perturbative limit of  
 643  $\frac{\gamma_e B}{D} \ll 1$ . We introduce the operators  $\hat{u}_\perp = \frac{\gamma_e B}{D} \sin \hat{\theta}$  and  $\hat{u}_\parallel = \frac{\gamma_e B}{D} \cos \hat{\theta}$ . Thus, we have  
 644  $\langle \hat{u}_\perp \rangle \ll 1$  and  $\langle \hat{u}_\parallel \rangle \ll 1$ . Using those operators, the Hamiltonian of the NV reads :

$$\hat{\mathcal{H}}'_{\text{NV}} = \hbar D \hat{S}_z^2 + \hbar D (\hat{u}_\parallel \hat{S}_z - \hat{u}_\perp \hat{S}_x) \quad (\text{A7})$$

<sup>645</sup> We can treat the second part of this Hamiltonian as a perturbation. We want to  
<sup>646</sup> move into the basis where this Hamiltonian is almost diagonal to second order in  $\frac{\gamma_e B}{D}$ .  
<sup>647</sup> We consider the unitary transformation :

$$\hat{U}'' = \begin{pmatrix} 1 - \frac{\hat{u}_\perp^2}{4} & \frac{\hat{u}_\perp}{\sqrt{2}}(1 - \hat{u}_\parallel) & -\frac{\hat{u}_\perp^2}{4} \\ -\frac{\hat{u}_\perp}{\sqrt{2}}(1 - \hat{u}_\parallel) & 1 - \frac{\hat{u}_\perp^2}{2} & -\frac{\hat{u}_\perp}{\sqrt{2}}(1 + \hat{u}_\parallel) \\ -\frac{\hat{u}_\perp^2}{4} & \frac{\hat{u}_\perp}{\sqrt{2}}(1 + \hat{u}_\parallel) & 1 - \frac{\hat{u}_\perp^2}{4} \end{pmatrix} \quad (\text{A8})$$

<sup>648</sup> The new states we are considering by applying this transformation are defined by  
<sup>649</sup> the equality to second order in  $\frac{\gamma_e B}{D}$  as :

$$|+1'\rangle = \left(1 - \frac{\hat{u}_\perp^2}{4}\right)|+1\rangle - \frac{\hat{u}_\perp}{\sqrt{2}}(1 - \hat{u}_\parallel)|0\rangle - \frac{\hat{u}_\perp^2}{4}| -1\rangle \quad (\text{A9})$$

$$|0'\rangle = \frac{\hat{u}_\perp}{\sqrt{2}}(1 - \hat{u}_\parallel)|+1\rangle + \left(1 - \frac{\hat{u}_\perp^2}{2}\right)|0\rangle + \frac{\hat{u}_\perp}{\sqrt{2}}(1 + \hat{u}_\parallel)| -1\rangle \quad (\text{A10})$$

$$|-1'\rangle = -\frac{\hat{u}_\perp^2}{4}|+1\rangle - \frac{\hat{u}_\perp}{\sqrt{2}}(1 + \hat{u}_\parallel)|0\rangle + \left(1 - \frac{\hat{u}_\perp^2}{4}\right)| -1\rangle \quad (\text{A11})$$

<sup>650</sup> We have the equality  $\hat{U}'^\dagger \hat{U}'' = \hat{I}d + o(||(\hat{u}_\perp, \hat{u}_\parallel)||^2)$  which means that  $\hat{U}''$  is unitary  
<sup>651</sup> to the second order in  $||(\hat{u}_\perp, \hat{u}_\parallel)||$ .

<sup>652</sup> Under this transformation, the NV Hamiltonian is then equal to :

$$\hat{\mathcal{H}}_{\text{NV}}'' \simeq \hbar D \begin{pmatrix} 1 + \hat{u}_\parallel + \frac{\hat{u}_\perp^2}{2} & 0 & \frac{\hat{u}_\perp^2}{2} \\ 0 & -\hat{u}_\perp^2 & 0 \\ \frac{\hat{u}_\perp^2}{2} & 0 & 1 - \hat{u}_\parallel + \frac{\hat{u}_\perp^2}{2} \end{pmatrix} \quad (\text{A12})$$

<sup>653</sup> which can be written in a clearer view as :

$$\hat{\mathcal{H}}_{\text{NV}}'' \simeq \hbar D \begin{pmatrix} 1 + \frac{\gamma_e B}{D} \cos \hat{\theta} + \left(\frac{\gamma_e B}{D}\right)^2 \frac{\sin \hat{\theta}^2}{2} & 0 & \left(\frac{\gamma_e B}{D}\right)^2 \frac{\sin \hat{\theta}^2}{2} \\ 0 & -\left(\frac{\gamma_e B}{D}\right)^2 \sin \hat{\theta}^2 & 0 \\ \left(\frac{\gamma_e B}{D}\right)^2 \frac{\sin \hat{\theta}^2}{2} & 0 & 1 - \frac{\gamma_e B}{D} \cos \hat{\theta} + \left(\frac{\gamma_e B}{D}\right)^2 \frac{\sin \hat{\theta}^2}{2} \end{pmatrix} \quad (\text{A13})$$

<sup>654</sup> Furthermore, we suppose that we are in an angular configuration where  $\langle \hat{u}_\perp \rangle \simeq$   
<sup>655</sup>  $\langle \hat{u}_\parallel \rangle$  which implies that  $\langle \sin \hat{\theta} \rangle^2 \ll \langle \cos \hat{\theta} \rangle$ . We can then neglect non diagonal terms in  
<sup>656</sup> this regime and we obtain a diagonal Hamiltonian :

$$\hat{\mathcal{H}}_{\text{NV}}'' \simeq \hbar D \begin{pmatrix} 1 + \frac{\gamma_e B}{D} \cos \hat{\theta} + \left(\frac{\gamma_e B}{D}\right)^2 \frac{\sin \hat{\theta}^2}{2} & 0 & 0 \\ 0 & -\left(\frac{\gamma_e B}{D}\right)^2 \sin \hat{\theta}^2 & 0 \\ 0 & 0 & 1 - \frac{\gamma_e B}{D} \cos \hat{\theta} + \left(\frac{\gamma_e B}{D}\right)^2 \frac{\sin \hat{\theta}^2}{2} \end{pmatrix} \quad (\text{A14})$$

**657 Appendix C.1.3 Moving to the equilibrium position of the Paul trap**

**658** We apply the unitary transformation  $\hat{U}''' = e^{i\theta' \hat{p}_\theta}$  which redefines  $\hat{\theta}$  as  $\hat{\theta} - \theta'$ . This  
**659** transformation doesn't affect the eigenstates of the spin and we obtain. To first order in  
**660**  $\hat{\theta}$  we can write :

$$\hat{\mathcal{H}}_{\text{NV}}''' \simeq \hbar(\omega_{+1} + G_{+1}\hat{\theta})|+1'\rangle\langle+1'| + \hbar(\omega_0 + G_0\hat{\theta})|0'\rangle\langle0'| + \hbar(\omega_{-1} + G_{-1}\hat{\theta})|-1'\rangle\langle-1'| \quad (\text{A15})$$

$$\omega_{+1} = D + \gamma_e B \cos(\theta') + \frac{(\gamma_e B)^2}{D} \frac{\sin(\theta')^2}{2} \quad (\text{A16})$$

$$\omega_0 = -\frac{(\gamma_e B)^2}{D} \sin(\theta')^2 \quad (\text{A17})$$

$$\omega_{-1} = D - \gamma_e B \cos(\theta') + \frac{(\gamma_e B)^2}{D} \frac{\sin(\theta')^2}{2} \quad (\text{A18})$$

$$G_{+1} = -\gamma_e B \sin(\theta') + \frac{(\gamma_e B)^2}{D} \frac{\sin(2\theta')}{2} \quad (\text{A19})$$

$$G_0 = -\frac{(\gamma_e B)^2}{D} \sin(2\theta') \quad (\text{A20})$$

$$G_{-1} = \gamma_e B \sin(\theta') + \frac{(\gamma_e B)^2}{D} \frac{\sin(2\theta')}{2} \quad (\text{A21})$$

**661 Appendix C.1.4 Moving to the rotating frame of the micro-wave**

**662** The last unitary transformation is to move into the micro-wave frame by doing the  
**663** unitary transformation  $\hat{U}'''' = e^{i\omega t \hat{S}_z^2}$ . This transformation is diagonal so it commutes  
**664** with the NV center Hamiltonian which is also diagonal. As it is a time-depending  
**665** transformation, this will add a shift in energy of both the  $|+1'\rangle$  and  $|-1'\rangle$  states which  
**666** gives the Hamiltonian :

$$\hat{\mathcal{H}}_{\text{NV}}'''' \simeq \hbar(\Delta_{+1} + G_{+1}\hat{\theta})|+1'\rangle\langle+1'| + \hbar(\Delta_0 + G_0\hat{\theta})|0'\rangle\langle0'| + \hbar(\Delta_{-1} + G_{-1}\hat{\theta})|-1'\rangle\langle-1'| \quad (\text{A22})$$

**667** by defining  $\Delta_{+1} = \omega_{+1} - \omega$ ,  $\Delta_{-1} = \omega_{-1} - \omega$  and  $\Delta_0 = \omega_0$ .

**668 Appendix C.2 Mechanical Hamiltonian transformation**

**669** In this section, we derive the calculation of the mechanical Hamiltonian. The initial  
**670** Hamiltonian reads :

$$\hat{\mathcal{H}}_{\text{mecha}} = \frac{\hat{p}_\theta^2}{2I} + \frac{1}{2} I \omega_\theta^2 (\hat{\theta} - \theta')^2 \quad (\text{A23})$$

**671 Appendix C.2.1 Moving to the particle frame**

**672** The unitary transformation  $\hat{U} = e^{i\hat{\theta}\hat{S}_y}$  changes the Hamiltonian into :

$$\hat{\mathcal{H}}'_{\text{mecha}} = \frac{(\hat{p}_\theta - \hbar\hat{S}_y)^2}{2I} + \frac{1}{2} I \omega_\theta^2 (\hat{\theta} - \theta')^2 \quad (\text{A24})$$

**673** In this frame,  $\hat{p}_\theta$  is defined as  $\hat{p}_\theta + \hbar\hat{S}_y$  which is the total angular momentum of the  
**674** system including the angular momentum of the spin.

<sup>675</sup> One of the assumption that we have made is to neglect non-inertial terms in the  
<sup>676</sup> Hamiltonian which means  $\hbar \langle \hat{S}_y \rangle \ll \langle \hat{p}_\theta \rangle$ . The Hamiltonian reads :

$$\hat{\mathcal{H}}'_{\text{mecha}} \simeq \frac{\hat{p}_\theta^2}{2I} + \frac{1}{2} I \omega_\theta^2 (\hat{\theta} - \theta')^2 \quad (\text{A25})$$

<sup>677</sup> Appendix C.2.2 Moving to the diagonalized basis of the NV Hamiltonian

<sup>678</sup> The unitary transformation  $\hat{U}''$  only depends on  $\hat{\theta}$  so it commutes with  $\hat{\theta}$ . This  
<sup>679</sup> transformation can be written  $\hat{U}'' = \hat{Id} + uV(\hat{\theta}) + o(|u|)$  with  $u = \frac{\gamma_e B}{D}$  and  $V(\hat{\theta}) =$   
<sup>680</sup>  $A \sin \hat{\theta}$  where  $A = \frac{1}{\sqrt{2}}(|+1\rangle\langle 0| - |0\rangle\langle +1| + |-1\rangle\langle 0| - |0\rangle\langle -1|)$ . Furthermore, we have  
<sup>681</sup>  $V(\hat{\theta})^\dagger = -V(\hat{\theta})$ . We have :

$$\hat{U}''^\dagger \hat{p}_\theta \hat{U}'' = (\hat{Id} - uV(\hat{\theta}) + o(|u|)) \hat{p}_\theta (\hat{Id} + uV(\hat{\theta}) + o(|u|)) \quad (\text{A26})$$

$$\hat{U}''^\dagger \hat{p}_\theta \hat{U}'' = \hat{p}_\theta + u [\hat{p}_\theta, V(\hat{\theta})] + o(|u|) \quad (\text{A27})$$

$$\hat{U}''^\dagger \hat{p}_\theta \hat{U}'' = \hat{p}_\theta + u A [\hat{p}_\theta, \sin \hat{\theta}] + o(|u|) \quad (\text{A28})$$

$$\hat{U}''^\dagger \hat{p}_\theta \hat{U}'' = \hat{p}_\theta - i\hbar u A \cos \hat{\theta} + o(|u|) \quad (\text{A29})$$

<sup>682</sup> We can safely neglect the second term under the initial assumption  $\langle \hat{p}_\theta \rangle \gg \hbar$ . Thus  
<sup>683</sup> we get:

$$\hat{\mathcal{H}}''_{\text{mecha}} \simeq \frac{\hat{p}_\theta^2}{2I} + \frac{1}{2} I \omega_\theta^2 (\hat{\theta} - \theta')^2 \quad (\text{A30})$$

<sup>684</sup> Appendix C.2.3 Moving to the stable position of the Paul trap

<sup>685</sup> This transformation changes the Hamiltonian into :

$$\hat{\mathcal{H}}'''_{\text{mecha}} \simeq \frac{\hat{p}_\theta^2}{2I} + \frac{1}{2} I \omega_\theta^2 \hat{\theta}^2 \quad (\text{A31})$$

<sup>686</sup> Appendix C.2.4 Moving to the rotating frame of the micro-wave

<sup>687</sup> This transformation doesn't affect the Hamiltonian of the mechanics :

$$\hat{\mathcal{H}}''''_{\text{mecha}} \simeq \frac{\hat{p}_\theta^2}{2I} + \frac{1}{2} I \omega_\theta^2 \hat{\theta}^2 \quad (\text{A32})$$

<sup>688</sup> Appendix C.3 Micro-wave Hamiltonian transformation

<sup>689</sup> In this section, we derive the calculation of the micro-wave Hamiltonian. The initial  
<sup>690</sup> Hamiltonian reads :

$$\hat{\mathcal{H}}_{\mu\text{w}} = \hbar \Omega \cos(\omega t) \hat{S}_x \quad (\text{A33})$$

<sup>691</sup> Appendix C.3.1 Moving to the particle frame

<sup>692</sup> This transformation changes the Hamiltonian into :

$$\hat{\mathcal{H}}'_{\mu w} = \hbar\Omega \cos(\omega t) (\cos \hat{\theta} \hat{S}_x + \sin \hat{\theta} \hat{S}_z) \quad (\text{A34})$$

<sup>693</sup> Appendix C.3.2 Moving to the diagonalized basis of the NV Hamiltonian

<sup>694</sup> This transformation doesn't change the Hamiltonian to first order in  $\frac{\gamma_e B}{D}$  :

$$\hat{\mathcal{H}}''_{\mu w} \simeq \hbar\Omega \cos(\omega t) (\cos \hat{\theta} \hat{S}_x + \sin \hat{\theta} \hat{S}_z) \quad (\text{A35})$$

<sup>695</sup> Appendix C.3.3 Moving to the stable position of the Paul trap

<sup>696</sup> This transformation changes the Hamiltonian into :

$$\hat{\mathcal{H}}'''_{\mu w} \simeq \hbar\Omega \cos(\omega t) (\cos(\theta' + \hat{\theta}) \hat{S}_x + \sin(\theta' + \hat{\theta}) \hat{S}_z) \quad (\text{A36})$$

<sup>697</sup> Appendix C.3.4 Moving to the rotating frame of the micro-wave

<sup>698</sup> Under the rotating-wave approximation and keeping only the first order term in  $\hat{\theta}$ ,  
<sup>699</sup> the Hamiltonian changes into :

$$\hat{\mathcal{H}}''''_{\mu w} \simeq \hbar \frac{\Omega}{2} \cos(\theta') \hat{S}_x \quad (\text{A37})$$

<sup>700</sup> Redefining  $\Omega = \Omega \cos(\theta')$ , we get :

$$\hat{\mathcal{H}}''''_{\mu w} \simeq \hbar \frac{\Omega}{2} \hat{S}_x \quad (\text{A38})$$

## <sup>701</sup> Appendix D Optical pumping in the new NV center eigenstates basis

<sup>702</sup> One may ask how the transformation into the new eigenstate basis affect the optical  
<sup>703</sup> pumping process which is less efficient in a presence of a transverse field.

<sup>704</sup> Calculs à mettre de changement de base avec les opérateurs lindbladiens ou alors  
<sup>705</sup> citer un papier qui traite de ça.

## References

1. Delić, U.; Reisenbauer, M.; Dare, K.; Grass, D.; Vuletić, V.; Kiesel, N.; Aspelmeyer, M. Motional Quantum Ground State of a Levitated Nanoparticle from Room Temperature. *ArXiv191104406 Phys. Physicsquant-Ph* **2019**, [[arXiv:physics, physics:quant-ph/1911.04406](#)].
2. Tebbenjohanns, F.; Frimmen, M.; Jain, V.; Windey, D.; Novotny, L. Motional Sideband Asymmetry of a Nanoparticle Optically Levitated in Free Space. *Phys. Rev. Lett.* **2020**, 124, 013603. doi:10.1103/PhysRevLett.124.013603.
3. Moore, D.C.; Geraci, A.A. Searching for New Physics Using Optically Levitated Sensors. *ArXiv200813197 Hep-Ex Physicshep-Ph Physicsphysics Physicsquant-Ph* **2020**, [[arXiv:hep-ex, physics:hep-ph, physics:physics, physics:quant-ph/2008.13197](#)].
4. Xiong, F.; Wu, T.; Leng, Y.; Li, R.; Duan, C.; Kong, X.; Huang, P.; Li, Z.; Gao, Y.; Rong, X.; Du, J. Searching Spin-Mass Interaction Using a Diamagnetic Levitated Magnetic Resonance Force Sensor. *ArXiv201014199 Quant-Ph* **2020**, [[arXiv:quant-ph/2010.14199](#)].
5. Vinante, A.; Carlesso, M.; Bassi, A.; Chiasera, A.; Varas, S.; Falferi, P.; Margesin, B.; Mezzena, R.; Ulbricht, H. Narrowing the Parameter Space of Collapse Models with Ultracold Layered Force Sensors. *Phys. Rev. Lett.* **2020**, 125, 100404. doi:10.1103/PhysRevLett.125.100404.
6. Gieseler, J.; Deutsch, B.; Quidant, R.; Novotny, L. Subkelvin Parametric Feedback Cooling of a Laser-Trapped Nanoparticle. *Phys. Rev. Lett.* **2012**, 109, 103603. doi:10.1103/PhysRevLett.109.103603.
7. Kiesel, N.; Blaser, F.; Delić, U.; Grass, D.; Kaltenbaek, R.; Aspelmeyer, M. Cavity Cooling of an Optically Levitated Submicron Particle. *PNAS* **2013**, 110, 14180–14185. doi:10.1073/pnas.1309167110.

8. Magrini, L.; Norte, R.A.; Riedinger, R.; Marinković, I.; Grass, D.; Delić, U.; Gröblacher, S.; Hong, S.; Aspelmeyer, M. Near-Field Coupling of a Levitated Nanoparticle to a Photonic Crystal Cavity. *Optica, OPTICA* **2018**, *5*, 1597–1602. doi:10.1364/OPTICA.5.001597.
9. Jones, P.H.; Marag-, O.M.; Volpe, G. *Optical Tweezers: Principles and Applications*, 1 edition ed.; Cambridge University Press: Cambridge, 2016.
10. Gieseler, J.; Kabcenell, A.; Rosenfeld, E.; Schaefer, J.D.; Safira, A.; Schuetz, M.J.A.; Gonzalez-Ballester, C.; Rusconi, C.C.; Romero-Isart, O.; Lukin, M.D. Single-Spin Magnetomechanics with Levitated Micromagnets. *Phys. Rev. Lett.* **2020**, *124*, 163604, [1912.10397]. doi:10.1103/PhysRevLett.124.163604.
11. Martinetz, L.; Hornberger, K.; Stickler, B.A. Gas-Induced Friction and Diffusion of Rigid Rotors. *Phys. Rev. E* **2018**, *97*, 052112. doi:10.1103/PhysRevE.97.052112.
12. Gieseler, J.; Novotny, L.; Quidant, R. Thermal Nonlinearities in a Nanomechanical Oscillator. *Nat Phys* **2013**, *9*, 806–810. doi:10.1038/nphys2798.
13. Conangla, G.P.; Nwaigwe, D.; Wehr, J.; Rica, R.A. Overdamped Dynamics of a Brownian Particle Levitated in a Paul Trap. *Phys. Rev. A* **2020**, *101*, 053823, [1912.11317]. doi:10.1103/PhysRevA.101.053823.
14. Arita, Y.; Mazilu, M.; Dholakia, K. Laser-Induced Rotation and Cooling of a Trapped Microgyroscope in Vacuum. *Nat. Commun.* **2013**, *4*, 2374. doi:10.1038/ncomms3374.
15. Hoang, T.M.; Ma, Y.; Ahn, J.; Bang, J.; Robicheaux, F.; Yin, Z.Q.; Li, T. Torsional Optomechanics of a Levitated Nonspherical Nanoparticle. *Phys. Rev. Lett.* **2016**, *117*, 123604. doi:10.1103/PhysRevLett.117.123604.
16. Reimann, R.; Doderer, M.; Hebestreit, E.; Diehl, R.; Frimmer, M.; Windey, D.; Tebbenjohanns, F.; Novotny, L. GHz Rotation of an Optically Trapped Nanoparticle in Vacuum. *Phys. Rev. Lett.* **2018**, *121*, 033602. doi:10.1103/PhysRevLett.121.033602.
17. Monteiro, F.; Ghosh, S.; van Assendelft, E.C.; Moore, D.C. Optical Rotation of Levitated Spheres in High Vacuum. *Phys. Rev. A* **2018**, *97*, 051802. doi:10.1103/PhysRevA.97.051802.
18. Ranjit, G.; Montoya, C.; Geraci, A.A. Cold Atoms as a Coolant for Levitated Optomechanical Systems. *Phys. Rev. A* **2015**, *91*, 013416. doi:10.1103/PhysRevA.91.013416.
19. Karg, T.M.; Gouraud, B.; Ngai, C.T.; Schmid, G.L.; Hammerer, K.; Treutlein, P. Light-Mediated Strong Coupling between a Mechanical Oscillator and Atomic Spins 1 Meter Apart. *Science* **2020**, *369*, 174–179. doi:10.1126/science.abb0328.
20. Thomas, R.A.; Parniak, M.; Østfeldt, C.; Møller, C.B.; Bærentsen, C.; Tsaturyan, Y.; Schliesser, A.; Appel, J.; Zeuthen, E.; Polzik, E.S. Entanglement between Distant Macroscopic Mechanical and Spin Systems. *Nat. Phys.* **2020**, pp. 1–6. doi:10.1038/s41567-020-1031-5.
21. Salakhutdinov, V.; Sondermann, M.; Carbone, L.; Giacobino, E.; Bramati, A.; Leuchs, G. Single Photons Emitted by Nanocrystals Optically Trapped in a Deep Parabolic Mirror. *Phys. Rev. Lett.* **2020**, *124*, 013607. doi:10.1103/PhysRevLett.124.013607.
22. Rahman, A.T.M.A.; Barker, P.F. Laser Refrigeration, Alignment and Rotation of Levitated Yb 3+ :YLF Nanocrystals. *Nat. Photonics* **2017**, *11*, 634. doi:10.1038/s41566-017-0005-3.
23. Pettit, R.M.; Neukirch, L.P.; Zhang, Y.; Vamivakas, A.N. Coherent Control of a Single Nitrogen-Vacancy Center Spin in Optically Levitated Nanodiamond. *J. Opt. Soc. Am. B, JOSAB* **2017**, *34*, C31–C35. doi:10.1364/JOSAB.34.000C31.
24. Delord, T.; Nicolas, L.; Schwab, L.; Hétet, G. Electron Spin Resonance from NV Centers in Diamonds Levitating in an Ion Trap. *New J. Phys.* **2017**, *19*, 033031, [1605.02953]. doi:10.1088/1367-2630/aa659c.
25. Hoang, T.M.; Ahn, J.; Bang, J.; Li, T. Electron Spin Control of Optically Levitated Nanodiamonds in Vacuum. *Nat Commun* **2016**, *7*, 12250. doi:10.1038/ncomms12250.
26. Rondin, L.; Tetienne, J.P.; Hingant, T.; Roch, J.F.; Maletinsky, P.; Jacques, V. Magnetometry with Nitrogen-Vacancy Defects in Diamond. *Rep. Prog. Phys.* **2014**, *77*, 056503. doi:10.1088/0034-4885/77/5/056503.
27. Tetienne, J.P.; Rondin, L.; Spinicelli, P.; Chipaux, M.; Debuisschert, T.; Roch, J.F.; Jacques, V. Magnetic-Field-Dependent Photodynamics of Single NV Defects in Diamond: An Application to Qualitative All-Optical Magnetic Imaging. *New J. Phys.* **2012**, *14*, 103033. doi:10.1088/1367-2630/14/10/103033.
28. Delord, T.; Huillery, P.; Nicolas, L.; Hétet, G. Spin-Cooling of the Motion of a Trapped Diamond. *Nature* **2020**, pp. 1–4, [1905.11509]. doi:10.1038/s41586-020-2133-z.
29. Horowitz, V.R.; Alemán, B.J.; Christle, D.J.; Cleland, A.N.; Awschalom, D.D. Electron Spin Resonance of Nitrogen-Vacancy Centers in Optically Trapped Nanodiamonds. *PNAS* **2012**, *109*, 13493–13497. doi:10.1073/pnas.1211311109.
30. Neukirch, L.P.; von Haartman, E.; Rosenholm, J.M.; Vamivakas, A.N. Multi-Dimensional Single-Spin Nano-Optomechanics with a Levitated Nanodiamond. *Nat Photon* **2015**, *9*, 653–657. doi:10.1038/nphoton.2015.162.